Micromagnetic analysis of exchange-coupled hard-soft planar nanocomposites

Giovanni Asti, Massimo Solzi, Massimo Ghidini, and Franco M. Neri
INFM and Dipartimento di Fisica dell'Università, Parco Area delle Scienze 7/A, I-43100 Parma, Italy
(Received 5 November 2003; revised manuscript received 13 February 2004; published 4 May 2004)

A complete magnetic phase diagram for exchange-coupled planar hard-soft nanocomposites has been obtained in the frame of a one-dimensional micromagnetic model describing the dependence of the properties along the growth direction. The phase diagram in terms of layer thicknesses provides information on the type of demagnetization processes and the critical fields at which nucleation and reversal take place. The basic criterion to this purpose is the analytical expression we have obtained of the critical susceptibility at the nucleation field. The phase diagram is divided into three regions: the exchange-spring magnet (ES), the rigid composite magnet (RM), and the decoupled magnet (DM). The main boundary line is an U-shaped line corresponding to divergence of the critical susceptibility. The diagram also reports the isocritical field lines both for the nucleation and the reversal field. These lines bifurcate along the RM boundary line. The essential characteristics of the phase diagram are directly connected with the intrinsic properties of the chosen soft and hard materials. With increasing ratio between the anisotropy constants of soft to hard phases the ES region is reduced until it disappears at a critical value. The model includes as limiting cases the classical problems of the planar soft inclusion in a bulk magnet and of the domain-wall depinning at the hard-soft interface.

DOI: 10.1103/PhysRevB.69.174401 PACS number(s): 75.50.Ww, 75.60.Jk, 75.60.Ej, 75.70.Cn

I. INTRODUCTION

In the present technological scenario the microsystem technologies are becoming more and more important with particular focus on microelectromechanical systems (MEMS) and micromachines. Typical applications are sensors, actuators, accelerometers, relays, bioMEMS, rfMEMS, and microfluidic and microwave devices. In this context the development of MEMS based on high performance permanent magnets is very promising. This goal has stimulated research towards the development of new concepts in permanent magnetism, without any constraints concerning the material cost. In recent years some attention has been devoted to composite magnets combining the best properties of a soft and a hard magnetic material via exchange coupling on a nanometric scale (exchange-spring magnet,[1] see Fig. 1 below). In particular it has been shown that oriented planar composite systems in the form of multilayers offer in principle the possibility of achieving the 1 MJ/m^3 theoretical limit for the energy density.[2,3] The *planar* magnetic nanocomposites are technologically relevant, at least in perspective. As an example, the millisize engines and microactuators have great potentialities in fields like bioengineering. Other applications could concern high-density magnetic recording and microwave integrated devices.

A multilayer is an intrinsically simple ideal system with an easily controllable and reproducible structure. In particular, thin-film growth allows the control of layer thickness and, in principle, it provides a mean for crystallographic alignment of the hard-phase easy axis. The dimensional scale parameter is the ferromagnetic exchange length l_{ex}, which can be considered as roughly proportional to the domain wall (DW) average thickness. In the case of very hard magnets, this quantity is only a few nanometers, while it is of the order of several tenths of nm for soft magnetic materials, such as α-Fe. In order to predict the macroscopic magnetic behavior of the exchange-spring magnet, Kneller *et al.*[1] proposed a qualitative one-dimensional model that takes into account the magnetostatic and exchange interactions among different crystallographically coherent grains. However, the magnetization reversal and coercivity mechanisms of real bulk systems certainly depend on the microstructural details, such as the three-dimensional spatial distribution of the two phases. On the other hand, the layered structures can be more properly modeled as one-dimensional structures, because they show variations in the magnetic properties predominantly along the growth direction. Therefore, an additional advantage of these systems is to allow a realistic estimate of the ultimate gain in performance that may potentially be realized

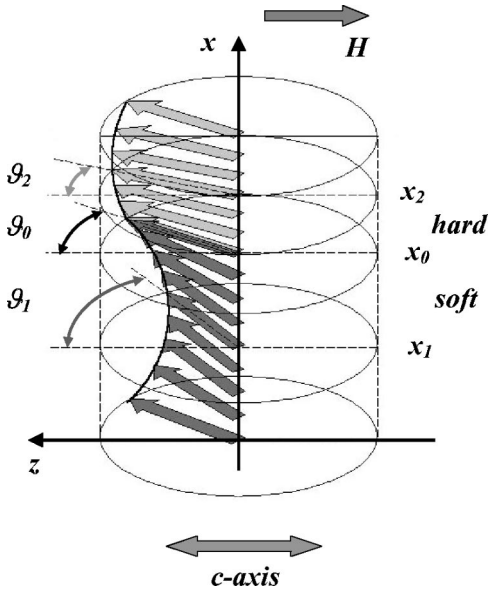

FIG. 1. Basic scheme for the one-dimensional micromagnetic continuum model of the planar hard-soft nanocomposite.

in exchange-spring bulk magnets.

Recent studies on hard/soft bilayers and multilayers (planar exchange-spring magnet) have shown that the flux reversal occurs in general in two stages beginning at well defined critical fields: the nucleation field H_{c1}, at which the magnetic moments start to deviate reversibly and nonuniformly from the easy direction; the reversal field H_{c2} that promotes the irreversible rotation of the whole system.

In order to gain a deep insight into the magnetization reversal process of the hard-soft composite magnet, we have developed a one-dimensional micromagnetic model and calculated the analytical expression of the differential susceptibility at the nucleation field. The dependence of this quantity on the structural parameters allows to define the magnetic phase diagram of the planar hard-soft composite. In this diagram, boundary critical lines separate the different regimes corresponding to distinct reversal mechanisms. The predictions of the model are here compared with existing experimental data and with the results of other theoretical analyses reported in the literature. The model, far from the nanometric scale, also includes important aspects of classic systems such as soft inclusions in a hard bulk. Finally some considerations are given concerning the best conditions for obtaining permanent magnets with the highest energy density. Before the presentation of our model, in Sec. II we give an overview of the main endeavors to realize permanent magnets in the form of planar magnetic nanocomposite systems, followed by a detailed analysis of the theoretical models especially developed to describe the magnetic behavior of these systems.

II. INTRODUCTORY OVERVIEW

The first attempts to realize a planar exchange-spring magnet focused on isotropic systems, either bilayers,[4,5] trilayers,[6,7] or multilayers,[8–10] constituted by Sm-Co or Nd-FeB as the hard phase and Fe, NiFe, and Co as the soft phase. Shi-Shen Yan *et al.*[11,12] studied extensively the $Ni_{80}Fe_{20}/Sm_{40}Fe_{60}$ system, by varying over a wide range both the hard- and the soft-layer thicknesses. Other authors followed a different approach, involving the growth of the nanocomposite thin films Co/Sm-Co (Ref. 13), Co/Pr-Co (Ref. 14), and Fe/FePt (Ref. 15), obtained by rapid thermal annealing of multilayered structures. In this case, the final two-phase nanostructured film shows the exchange-hardening behavior although keeping no trace of the original layered structure. These first endeavors have shown the feasibility of a multilayer nanocomposite magnet, but on the other hand, they have also stressed the difficulties existing on the way of achieving the ideal 1 MJ/m^3 magnet,[2,3] e.g., the interfacial roughness, which can influence the exchange coupling between layers[6] and the alignment of their easy axes.

An attempt to overcome the latter problem was the epitaxial growth of Co/Sm-Co and Fe/Sm-Co bilayers obtained by sputtering deposition.[16] In principle, the stacking of bilayers of this type should produce a soft/hard multilayer having essentially the same properties of the component bilayer, if the reversal process occurs homogeneously. However, the growth of multilayers of this kind seems now not so straightforward,[17] although there are some attempts to realize Co/Sm-Co superlattices.[10,17] From a different point of view, other authors explored the possibility of modulating the intensity of interfacial exchange, by exploiting the phenomenon of interdiffusion between Co/CoPt bilayers.[18,19] Following a different approach, thin-film nanocomposite magnets were obtained by randomly dispersing soft-inclusions in an oriented hard matrix.[20,21]

Starting from a different viewpoint, Asti *et al.*[22–24] realized a model system constituted by alternate layers of simple materials (elemental Fe and Co) but with special care for the interface condition. For this purpose, they have employed ultra high-vacuum deposition techniques (electron-beam evaporation) with very low deposition rates to obtain clean and sharp interfaces. Furthermore, they have investigated the effect of the layer thickness on the structural and magnetic properties of Fe/Co multilayers having a constant number of layers and a given Fe/Co thickness ratio. The obtained systems show a single-phase-like behavior (almost bistable) with a steep magnetic reversal. The recoil susceptibility of all the studied multilayers approaches the slope of the major loop at remanence, as in a classical permanent magnet.

III. THEORETICAL MODELS

The literature on the theory of magnetization reversal in multilayered exchange-coupled thin film structures can be classified by the following scheme: (i) continuum-approach micromagnetic models,[25–27] which allow one to deduce analytic expressions of relevant parameters, (ii) discrete models[16,28,29] that are useful for very thin films, (iii) computational approaches based on solving the dynamic equation of motion,[30,31] and (iv) first-principles calculations, aimed at determining the band-energy structure.[32]

The inhomogeneous distribution of the magnetization is generally to be expected in such a manner that at equilibrium the magnetization is always parallel to the film plane and thus the problem can be considered as one dimensional along an axis perpendicular to the multilayer plane. As a consequence of the chosen in-plane distribution of the magnetic moments, corresponding to Bloch-wall-type configurations, the stray fields are vanishing.

A. Continuum models

The use of the continuum approximation for the multilayer problem is justified down to thicknesses of a few atomic layers.[25,27] Within this approach, models have been mainly utilized to deduce analytically the instability field in some special cases, such as the two-coupled-layers problem, first addressed by Goto *et al.*[25] In their model, the spin configuration inside the isotropic soft layer corresponds to a continuous rotation, as in Bloch walls. The spins in the hard substrate with infinite anisotropy are assumed to remain parallel, therefore imposing the boundary condition to the soft-layer magnetization. Through the analytical solution of the Euler equation, Goto *et al.*[25] deduce the shape of the theoretical magnetization curve. In particular, they express the angular distribution of magnetization vector in the soft layer in

terms of Jacobi elliptic functions. They individuate a critical value of the field (instability field, usually called the exchange-bias field) corresponding to the initial deviation of the spins in the soft layer from the parallelism with respect to the spins of hard layer. This field is inversely proportional to the squared soft-layer thickness. The same authors also considered the more general case of two exchange-coupled films with different uniaxial anisotropy,[25] but did not explicitly reduce the problem to a set of elliptic integrals, due to the complexity of mathematical expressions. They deduced instead approximate solutions in special cases,[33,34] such as, the limit of vanishing hard-layer thickness with infinite anisotropy (degenerate hard film), with the condition of a constant thickness-anisotropy product.[25] Hagedorn[26] further developed the above model by investigating the stability of equilibrium magnetic configurations by deducing an analytical expression for the second variation of the magnetic energy, which he evaluated through numerical calculations.

The background of the above-described approach is the problem of calculating the nucleation field of a ferromagnetic crystal with inclusions having lower uniaxial magnetocrystalline anisotropy.[35,36] For example, a one-dimensional model was developed by Aharoni,[35] in which a crystal extending infinitely in all directions is considered, including a zero-anisotropy slab of finite width. The procedure to obtain an analytical expression for the nucleation field essentially relies on the solution of the linearized Brown's equations. A further evolution of these models was proposed by Abraham,[37] where a bulk crystal is covered by a surface layer having zero anisotropy, but different exchange and magnetization.

In recent years Leineweber and Kronmüller[27,38] examined the case of a soft layer with finite thickness sandwiched between two infinite hard layers. They derived expressions for the angular orientation of the magnetization vector throughout the layers, both with and without an applied magnetizing field, as a function of the intrinsic (exchange, magnetocrystalline anisotropy) and extrinsic (thickness) characteristics of the layers. On the basis of these results, the authors deduced the remanence, reversal field and maximum energy product of the triple-layer system. They calculated the reversal field (they called this field ''nucleation field'' H_n) as a function of the soft-layer half-thickness (therein denoted d_s) and deduced that this critical field coincides with the hard-layer anisotropy field, if $2d_s$ is below the *hard* Bloch wall thickness $\pi\delta_h = \pi\sqrt{A_h/K_h}$. In this region, the value of H_n does not depend on the particular d_s value, and the system can develop a complete exchange coupling between the two phases. Furthermore the hysteresis loop is rectangular as in the case of a pure hard bulk, with only one critical field, and the magnetization reversal is only due to a rotation mechanism. A different behavior is instead deduced if $2d_s$ is of the order of one or a few $\pi\delta_h$, when H_n turns out to decrease steeply with increasing d_s. This situation corresponds to the so-called exchange-coupled phase,[38] in which an inhomogeneous (irreversible) rotation mechanism predominates the magnetization reversal, following a reversible process caused by the exchange coupling. The hysteresis loop is no more rectangular in shape and one can distinguish a first critical field, at which the collinearity is broken and the reversible process starts (the exchange-bias field), and a second critical field corresponding to the irreversible switch of the whole system. The hysteresis behavior of the system can be considered as a single-phase magnetic behavior. On the contrary, in the extreme case, corresponding to $2d_s \gg \pi\delta_h$, the hard and soft phase can be considered as decoupled and the hysteresis cycle is typical of a two-phase system, with two different reversal fields. In this region, the magnetization reversal takes place by rotation of the moments independently and irreversibly in the hard and soft phases and the hard-phase reversal field decreases with an inverse power of d_s.

A remarkably different analytical approach is that based on the analogy between quantum mechanics and micromagnetics.[39,40] In essence, the micromagnetic equation which is obtained by the minimization of free energy corresponds to the Schrödinger's equation for a particle moving in a three-dimensional potential of the form $2K_1(r)/\mu_0 M(r)$. In particular the treatment of the multilayer limit is analogous to the periodic multiple quantum well problem (one dimensional), leading to the implicit equation for the nucleation field [see Eq. (A11)] as a function of hard and soft-layer thicknesses and of intrinsic parameters of the two phases.[39] At this place we should also cite an earlier treatment of the problem of inhomogeneous nucleation in periodic hard-soft multilayers based on the Kronig-Penney model,[41] allowing the derivation of the linearized micromagnetic equation as a one-dimensional Schrödinger's equation.

B. Other models

The micromagnetic approach suffers of some limitations, partly because the complete solution of the variational problem is possible only by approximation and numerical methods, and partly because it is based on a continuum model of matter, which becomes inaccurate when the layers thickness is very small. The discrete models assume the one-dimensional character of the reversal mode and have been applied to explain the observed magnetic behavior of exchange-spring bilayers,[16,17,29,42] triple-layers,[43] and multilayers.[29,42] The basic assumption is that the magnetic properties are considered to be constant within a ''sheet'' or ''layer'' parallel to the interfaces and to depend only on a plane index *i*, which corresponds to the coordinate perpendicular to the planes. Most authors assume that such layers are separated by a distance equal to the lattice parameter. In these models the coupling only occurs between neighboring ''layers'' and may be described, e.g., by an energy per unit surface area.[28] On this basis Amato *et al.*[29] demonstrated that on increasing the nanostructuration of the multilayer, that is, on increasing the number of alternate layers while keeping constant the total thickness and the hard/soft ratio, both the coercivity field and the maximum energy product are enhanced.

A different approach is based on the magnetodynamic Landau-Lifshitz equation for distributed ferromagnetic film systems.[30,31] The explicit purpose of the authors was to overcome the complications of the quasistatic description (mainly concerning the verification of the stability of the solutions

obtained from energy minimization) in the case of distributed systems such as films with laminar magnetization. The authors claim the dynamic solutions to be less complicate and more convenient, even including the problem of stability.

IV. THE ADOPTED MODEL

Following the guidelines of the micromagnetic approach, we handled the problem of the physical existence of the solutions arising from variational calculus by utilizing an heuristic viewpoint, essentially based on the study of the magnetic susceptibility in correspondence to the critical fields.[44] We calculated indeed the analytical expression of the differential susceptibility (χ_c) at the critical field that corresponds to the start of flux reversal (hereafter called nucleation field H_{c1}, as usual in the micromagnetic treatment[45]), on the basis of a one-dimensional micromagnetic model of the exchange-spring multilayer. The value of χ_c is an important parameter characterizing the type of reversal process and it is of particular interest the evaluation of its dependence on the properties of the soft and the hard phases and on structural parameters.

The adopted model considers the exchange-spring multilayer as composed by alternate soft and hard layers perpendicular to the x axis (see the scheme in Fig. 1). The two component layers are supposed to have uniaxial anisotropy with parallel easy axes both lying in the film plane along the z axis (Fig. 1). The search for solutions is limited to those which are periodical, so that the median planes of the layers are symmetry planes for the magnetic structure. The proposed approach is (i) based on a continuum model of matter, (ii) it does not take explicitly into account temperature effects, except for the fact they are implicit in the magnetic parameters normally utilized in a micromagnetic treatment, (iii) it also neglects the time dependence of magnetization, thus considering a quasistatic magnetization reversal, and (iv) it does not consider the possible contribution of surface and interface anisotropy. In the case of an applied magnetic field H opposite to the z axis, the expression of the Gibbs free energy can be written as

$$G=\sum_{i=1,2}(-1)^i\int_{x_0}^{x_i}\left[A_i\left(\frac{d\vartheta}{dx}\right)^2+\mu_0 M_i H\cos\vartheta+K_i\sin^2\vartheta\right]dx, \tag{1}$$

where indexes 1 and 2 refer to the soft and hard layer, respectively, and x_0, x_1, and x_2 denote the position of the interface and of two contiguous median planes (Fig. 1), $\vartheta(x)$ is the angle between the z axis and the magnetization vector $\mathbf{M}$, and A_i is the exchange stiffness constant of layer i. The magnetocrystalline anisotropy term is limited to the second order. We also define the quantities $t_1=(x_0-x_1)$, $t_2=(x_2-x_0)$, which represent half of the respective layer thicknesses.

The magnetization of both layers is supposed to lie generally in the film plane. Hence in Eq. (1) no demagnetizing field contribution to the free energy has been taken into account. In the case of an exchange-coupled multilayer with perpendicular anisotropy, a further energy contribution due to stray fields should be introduced into the model in form of a demagnetizing anisotropy constant for each layer ($K_i^{\mathrm{dm}}=\mu_0 M_i^2/2$). In this case the magnetic field is applied antiparallel to the x axis and the intrinsic anisotropy constants K_i should be substituted by the corresponding total anisotropy constants $L_i=K_i-\mu_0 M_i^2/2$, where a positive K_i indicates that the x axis is an easy axis. A further assumption is that $\mathbf{M}_i$ in both layers lies in the xy plane and the angle ϑ is the orientation angle of $\mathbf{M}_i$ with respect to the positive direction of x axis. This means that the problem has again a one-dimensional character with one degree of freedom (y component of $\mathbf{M}_i$) and the mathematical treatment presented below also applies to the case of perpendicular anisotropy. In particular, in the limit $K_1=K_2$, $M_1=M_2$, the system reduces to a classic infinite slab with perpendicular anisotropy (see Ref. 45, p. 194). Our assumptions are consistent with this case characterized by a spin reversal triggered by the nucleation of a uniform rotation mode at a critical field $H_c=(2K-\mu_0 M^2)/\mu_0 M$ (Ref. 46). So we expect that the one-dimensional approach we utilize in the model is also appropriate for describing the nucleation process in the exchange-coupled multilayer with remanent saturated state perpendicular to the film plane. However this description could be no more adequate in the region far from saturation. In particular the second critical field H_{c2}, at which the complete reversal of the whole system occurs, could substantially differ from the values predicted by the model because the system could take advantage of the additional degree of freedom (z component of $\mathbf{M}_i$).

The determination of equilibrium state is a variational problem. In this particular case, one has to consider the periodic boundary conditions $(d\vartheta/dx)=0$ for $x=x_1$ and $x=x_2$ and $A_1(d\vartheta/dx)|_{x=x_0-}=A_2(d\vartheta/dx)|_{x=x_0+}$ for $x=x_0$. The last condition corresponds to the Weierstrass-Erdmann law along the surface normal, which is also cited in Ref. 27. The absence of an explicit dependence on x of the integrand allows to directly obtain from the Euler equation a first order integral, which reads

$$\mu_0 M_i H(\cos\vartheta-\cos\vartheta_i)+K_i\sin^2\vartheta-A_i\left(\frac{d\vartheta}{dx}\right)^2-K_i\sin^2\vartheta_i=0, \tag{2}$$

from which

$$\frac{d\vartheta}{dx}=\sqrt{\alpha_i(\cos\vartheta-\cos\vartheta_i)+\beta_i(\sin^2\vartheta-\sin^2\vartheta_i)}, \tag{3}$$

where $i=1$ for $x_1<x<x_0$ and $i=2$ for $x_0<x<x_2$ and $\alpha_i=\mu_0 M_i H/A_i$, $\beta_i=K_i/A_i$. The boundary angles are ϑ_i for $x=x_i$ and ϑ_0 for $x=x_0$. Because we are interested in the

behavior for small angular deviations around the field H_{c1}, Eqs. (3) are then expanded up to the fourth order in ϑ and become

$$\frac{d\vartheta}{\sqrt{|\vartheta^2-\vartheta_i^2|}}\left[1+\frac{p_i}{2}(\vartheta^2+\vartheta_i^2)\right]=dx\sqrt{\left|\beta_i-\frac{\alpha_i}{2}\right|}, \quad (4)$$

where

$$p_1=\frac{\alpha_1-8\beta_1}{12(2\beta_1-\alpha_1)},$$

$$p_2=\frac{\alpha_2-8\beta_2}{12(\alpha_2-2\beta_2)}. \quad (5)$$

In Eqs. (4), the argument of the modulus has negative sign for the soft layer ($\vartheta<\vartheta_1$) and positive sign for the hard layer ($\vartheta>\vartheta_2$). The obtained equations are then integrated between the extrema, which are $\vartheta=\vartheta_1$ and $\vartheta=\vartheta_0$ for the soft layer, $\vartheta=\vartheta_0$ and $\vartheta=\vartheta_2$ for the hard layer, and the corresponding values for variable x (see Ref. 47).

Then we obtain two linear equations for the soft and the hard layer in terms of higher order infinitesimal variables η_j ($j=0,1,2$) that define the deviations of angles ϑ_j from their unperturbed values corresponding to the onset of instability at $H=H_{c1}$. The magnetic field itself is expressed in terms of an infinitesimal reduced variable $\tau=(H-H_{c1})/H_{c1}$, that vanishes when $H=H_{c1}$ (see Appendix A). A third equation is obtained by considering the boundary condition at $x=x_0$, which corresponds to the equilibrium condition for the exchange forces. Thus we obtain a system of three linear equations in the angles η_j. At $H=H_{c1}$ (i.e., $\tau=0$) it becomes a system of homogeneous linear equations: the condition is that the determinant Δ of the coefficient matrix is vanishing, leading to an implicit equation for the critical field H_{c1} (see Appendix A). For $\tau\neq 0$ a mathematical relation is obtained between the infinitesimal field τ and angles ϑ_j [see Eq. (A10)], which in turn allows to obtain an expression of the slope of $M(H)$ at the nucleation field H_{c1}.

Appendix B reports the calculation of the infinitesimal decrease of the reduced magnetization, $\delta m=\delta M/M_s$ (M_s is the saturation magnetization of the whole system) which is proportional to ϑ_0^2 through a factor Γ, which is a function of the layer thicknesses and the magnetic parameters. Then the reduced susceptibility is [Appendix B, Eq. (B5)]

$$\tilde{\chi}=\frac{\delta m}{\tau}=\frac{\vartheta_0^2\Gamma}{\tau}. \quad (6)$$

Equation (A10) of Appendix A yields the ratio ϑ_0^2/τ and thus the volume susceptibility at the critical field H_{c1} (in SI units) turns out to be

$$\chi_c=\frac{\delta M}{\delta H}=\frac{\delta m M_s}{(H-H_{c1})}=\frac{\vartheta_0^2\Gamma M_s}{H_{c1}\tau}=\tilde{\chi}\frac{M_s}{H_{c1}} \quad (7)$$

or, equivalently,[44]

$$\chi_c=\left\{\frac{M_1\left[\frac{t_1}{\cos^2(t_1\gamma_1)}+\frac{\tan(t_1\gamma_1)}{\gamma_1}\right]+M_2\left[\frac{t_2}{\cosh^2(t_2\gamma_2)}+\frac{\tanh(t_2\gamma_2)}{\gamma_2}\right]}{\frac{3p_1}{\cos^2(t_1\gamma_1)}\left[\frac{2t_1\gamma_1}{\sin(2t_1\gamma_1)}+1\right]-\frac{3p_2}{\cosh^2(t_2\gamma_2)}\left[\frac{2t_2\gamma_2}{\sinh(2t_2\gamma_2)}+1\right]+2(p_1-p_2)}\right\}$$
$$\times\left\{\alpha_1\left[\frac{1}{\gamma_1^2}+\frac{2t_1}{\gamma_1\sin(2t_1\gamma_1)}\right]+\alpha_2\left[\frac{1}{\gamma_2^2}+\frac{2t_2}{\gamma_2\sinh(2t_2\gamma_2)}\right]\right\}\cdot\left[\frac{1}{4H_{c1}(t_1+t_2)}\right], \quad (8)$$

where γ_1 and γ_2 are defined in Appendix A as functions of α and β.

V. THE MAGNETIC PHASE DIAGRAM

The dependence of χ_c on the structural parameters allows to define a phase diagram in the (t_1,t_2) plane. Figure 2 represents the phase diagram of a typical exchange-spring multilayer, calculated for the case of a Fe/Sm-Co system, with the same layer intrinsic parameters already utilized by Fullerton *et al.*[16] ($M_1=1.7$ MA/m, $M_2=0.55$ MA/m, $K_1=10^2$ J/m^3, $K_2=5$ MJ/m^3, $A_1=2.8\times10^{-11}$ J/m, and $A_2=1.2\times10^{-11}$ J/m). Starting from the thick layers region, the critical susceptibility is positive and increases continuously when reducing the half-layer thickness t_1 and t_2, until χ_c diverges along a critical line ($\chi_c\to\infty$). This line corresponds to the onset of instability and, in the region below it, χ_c becomes negative, indicating that the flux reversal occurs irreversibly. This critical condition separates the regime of the so-called exchange-spring magnet (ES, $\chi_c>0$) from that of the magnetically rigid composite magnet (RM, $\chi_c<0$), which is very similar to a conventional oriented magnet. In the latter, the reversible portion of the demagnetization curve on the left of H_{c1} (usually interpreted to be indicative of ''exchange-spring behavior'') is absent.

The first critical field H_{c1} is the solution of the implicit equation (A11) of Appendix A. Given t_1 and t_2, this is an equation in H through γ_1 and γ_2, and it is usually solved by using the simple method of bisection (see Ref. 48, p. 353). In

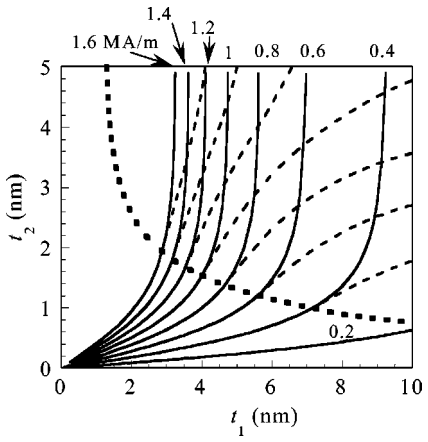

FIG. 2. Magnetic phase diagram in the plane of half-layer thicknesses t_1 (soft) and t_2 (hard) for the case of a Fe/Sm-Co multilayer, with parameters $M_1=1.7$ MA/m, $M_2=0.55$ MA/m, $K_1=10^2$ J/m^3, $K_2=5$ MJ/m^3, $A_1=2.8\times10^{-11}$ J/m, $A_2=1.2\times10^{-11}$ J/m (from Ref. 16). The figure reports the critical χ_∞ line ($\chi_c\to\infty$, dotted line) together with the lines of constant critical field H_{c1} (solid) and H_{c2} (dashed).

this way the H_{c1} lines have been traced on the magnetic phase diagram. The curves corresponding to constant values of the critical susceptibility χ_c in the (t_1,t_2) plane are found by a similar method: given t_1, we find the corresponding point of the iso-χ_c curve with the bisection, by letting t_2 vary. Since expression (8) for χ_c also depends on H_{c1}, we have to solve equation (A11) for each step of the bisection. In order to trace the H_{c2} curves, we first have to calculate the demagnetization curves (see Appendix C). The condition to determine this critical field is the divergence of the reversible susceptibility, a criterion discussed in detail by Hubert and Rave.[49]

The lines of constant critical fields H_{c1} and H_{c2} are presented in Fig. 2 over the half-layer thicknesses t_1 and t_2, together with the line of constant critical susceptibility $\chi_c\to\infty$ (χ_∞ line), which separates the RM regime from the ES regime. In the RM regime the isocritical field lines for H_{c1} and H_{c2} coincide, while there is a bifurcation of these lines on the χ_∞ line and a separation in the ES region. With the material parameters used, the RM region corresponds to rather small thicknesses for both layers, of the order of a few nm. In general, by setting a specific value of the soft-layer half-thickness t_1, H_{c1} becomes larger by increasing t_2. However, due to the fact that the H_{c1} lines show a vertical asymptote, by increasing the hard-layer thickness beyond a certain value, H_{c1} changes no more.

Another system that has been proposed as a possible exchange-coupled planar composite is Fe/NdFeB. The phase diagram for a Fe/NdFeB infinite multilayer is shown in Fig. 3(a), based on the material parameters given in Ref. 27 ($M_1=1.7$ MA/m, $M_2=1.28$ MA/m, $K_1=4.3\times10^4$ J/m^3, $K_2=4.3$ MJ/m^3, $A_1=2.5\times10^{-11}$ J/m, $A_2=7.7\times10^{-12}$ J/m). If we extend the phase diagram to the region of large soft half-layer thicknesses [Fig. 3(a)], we observe that the χ_∞ line assumes a typical U shape. This line presents two vertical asymptotes, corresponding to particular values

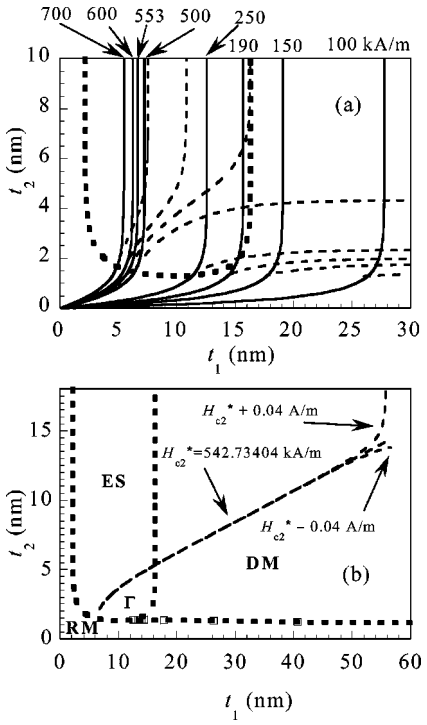

FIG. 3. (a) Fe/NdFeB composite system (data from Ref. 27): magnetic phase diagram in the plane of half-layer thicknesses t_1 (soft) and t_2 (hard). The U-shaped dotted line represents the critical χ_∞ line ($\chi_c\to\infty$). The figure also reports the H_{c1} (solid) and H_{c2} lines (dashed), which coincide in the RM region (left-bottom side of the diagram). (b) Same as (a) but with an enlarged scale, in order to give evidence to the H_{c2}^* line corresponding to the value 542.73404 kA/m: this line discriminates the H_{c2} lines having a vertical asymptote from those having horizontal asymptote (two examples are traced on the diagram, see text). The figure also shows the different regions in which the U-shaped critical line and the bifurcation line subdivide the phase diagram. The bifurcation line (dotted line) denotes the boundary between coupled and decoupled systems.

of the soft-layer thickness. As a consequence, if we focus the attention to the case of relatively large hard-layer thicknesses, the phase diagram is subdivided into three regions. (1) On the left of first asymptote, the system is in the RM regime dominated by the hard phase, that is, with large critical fields. (2) On the right of the second asymptote, the system is in a decoupled regime [decoupled magnet (DM)], where the hard and soft phases behave as almost independent components. (3) The intermediate region pertains to the usual ES regime. In the decoupled region the nucleation field H_{c1} does not mark the starting of a reversible detachment of the magnetic moments from saturated state: it indicates instead the occurrence of the irreversible switching of the soft phase, which is followed by a similar process involving the hard phase at the field H_{c2}. The corresponding demagnetization curve is typical of a two-phase system, as prefigured in Refs. 1 and 38. For Fe/Sm-Co system, the second asymptote occurs at very large t_1 values (of the order of 200 nm).

Figure 3(a) also reports the iso-critical lines corresponding to the reversal field H_{c2}. Note that those lines corre-

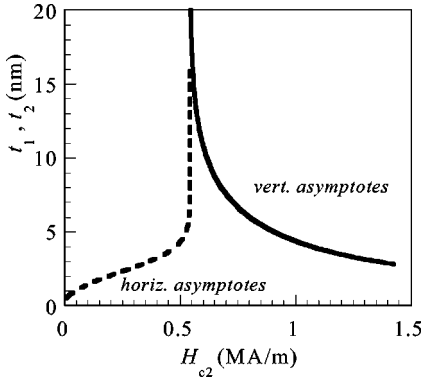

FIG. 4. Fe/NdFeB composite system (data from Ref. 27): hard-layer half-thickness position t_2 of the horizontal asymptotes for the H_{c2} lines, as a function of the H_{c2} value. On the same figure it is also reported the soft-layer half-thickness position t_1 of the vertical asymptotes for the H_{c2} lines. The discontinuity corresponds to the critical field $H_{c2}^{*}=542.7340384$ kA/m (see Fig. 3).

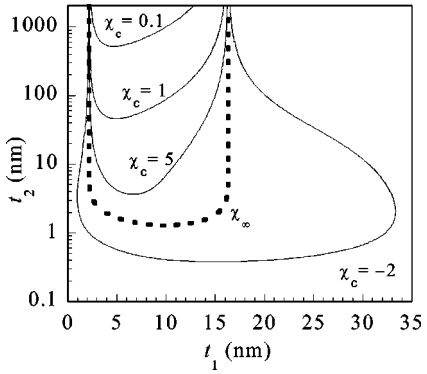

FIG. 5. Fe/NdFeB composite system (data from Ref. 27): magnetic phase diagram in the plane of half-layer thicknesses t_1 (soft) and t_2 (hard). On the diagram the U-shaped dotted line represents the χ_∞ line, and the other lines (solid) are isocritical susceptibility lines. The hard-layer thickness scale is logarithmic.

sponding to fields above a specific value H_{c2}^{*} show a vertical asymptote, while those referring to a field lower than H_{c2}^{*} present a horizontal asymptote. This critical field value ($H_{c2}^{*}=542.73404$ kA/m with the utilized material parameters) can be obtained by imposing that both layer thicknesses are infinite: the corresponding iso-H_{c2} curve appears to have an oblique asymptote in the region of large thicknesses. It is worth noting [Fig. 3(b)] that a very small change of this critical field value H_{c2}^{*} in either directions, even on the eighth digit ($H_{c2}^{*}\pm 0.04$ A/m), gives rise to isocritical field curves that are practically coincident up to a certain point, where they bifurcate taking either a vertical or an horizontal asymptote. Figure 4 reports the calculated thickness positions of the horizontal and vertical asymptotes, respectively, as a function of the critical field H_{c2}. The divergence of both curves occurs at the critical field value H_{c2}^{*}.

Another peculiar characteristic of the obtained phase diagram, as can be seen from Fig. 3(a), is that the bifurcation of the H_{c1} and H_{c2} lines occurs exactly in correspondence to the critical line χ_∞ only for fields above a specific value (about 210 kA/m, with the utilized material parameters). For fields lower than this value, the bifurcation occurs along a line that branches out of the critical line χ_∞. This "detachment" of the bifurcation from the χ_∞ critical line can be visualized by plotting on the phase diagram the bifurcation points corresponding to different field values, as it can be deduced from Fig. 3(a). One obtains thus a critical line [Fig. 3(b)], called the bifurcation line, which is nearly horizontal and denotes the boundary between coupled and decoupled systems. Below this line the system is exchange coupled: in particular it is a rigid magnet dominated by the soft phase, that is, with small critical fields. Above the bifurcation the hard and soft phases behave as nearly independent components (DM regime). The bifurcation line converges into the left-hand side of the U-shaped critical line to a tri-critical point Γ. The definition of the decoupled magnet is inherently subject to certain arbitrariness. We have considered in the present analysis a decoupled system as the one for which $|H_{c1}|\leqslant|H_{c2}|$ while $\chi_c<0$. Another possible definition could be connected with the introduction of a third critical field at which the irreversible transition occurs when the saturated and the intermediate states have equal free energy. In this case we could have again a two-step demagnetization curve in the region where $|H_{c1}|>|H_{c2}|$ and the new bifurcation line would be shifted to lower t_2 values while converging on the same tricritical point Γ.

Figure 5 shows the isocritical susceptibility lines superimposed to the magnetic phase diagram of the Fe/NdFeB infinite multilayer, with the hard-layer thickness on a logarithmic scale, in order to put in evidence the peculiar behavior in the limit of very large hard-layer thickness. In this limit, the iso-χ_c lines are still open lines and tend to concentrate close to the U-shaped critical line. This means that for very thick hard-layer thicknesses, the critical susceptibility of composite system is practically zero for all soft-layer thicknesses, except in a very narrow region around the vertical asymptotes, where it diverges. This fact reflects the obvious circumstance that χ_c is a weighted average of the susceptibility contribution of both components (hard and soft). With increasing hard-layer thickness the demagnetization pattern tends to be invariant and involves the same volume, which is a decreasing fraction of the whole system.

VI. DEPENDENCE OF THE MAGNETIC PHASE DIAGRAM ON MATERIAL PARAMETERS

Let us examine first the effect of an increasing soft-layer anisotropy on the phase diagram. Starting from the anisotropy ratio $\rho=K_1^{*}/K_2$ as in the case of Fig. 2 (Fe/Sm-Co), the phase diagram modifies as shown in Fig. 6(a). The two asymptotes of the critical line χ_∞ approach one another on increasing ρ, until they meet for a particular value ρ' (for soft/Sm-Co it is about 0.06, while in the case of the soft/NdFeB multilayer it is 0.034), so that the region of existence of the ES magnet vanishes. So the U-shaped curve collapses in a half-line starting from the tricritical point Γ, where it links up with the bifurcation line thus forming a unique new

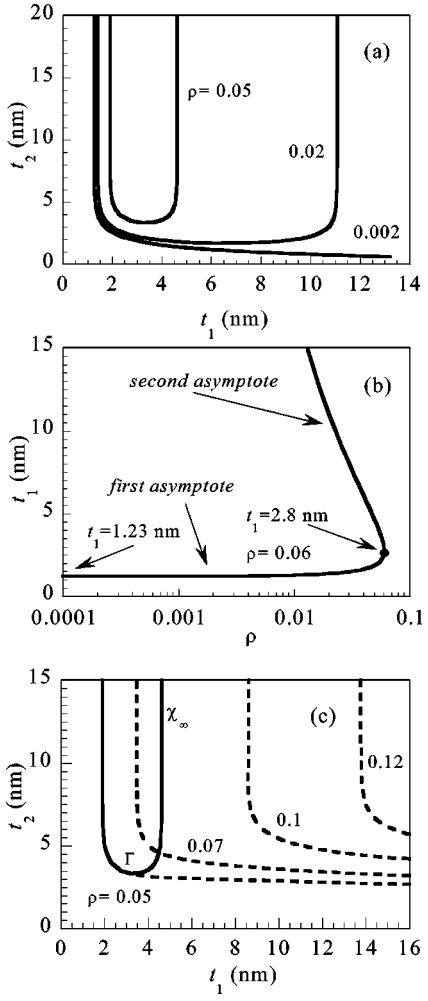

FIG. 6. Soft/Sm-Co composite system (starting data from Ref. 16): (a) modification of the χ_∞ line in the magnetic phase diagram on varying the $\rho = K_1^*/K_2$ ratio, with fixed K_2. (b) Soft-phase half-thickness position of first and second asymptotes of the χ_∞ line as a function of ρ. The position $t_1 = 1.23$ nm represents the limit for $K_1 \to 0$. The two asymptotes coalesce at a critical ratio $\rho = \rho' = 0.06$, corresponding to $t_1 = 2.8$ nm: for higher values of ρ the ES phase disappears. (c) Phase diagram for $\rho > \rho'$ (broken lines represent the new boundary lines separating RM and DM phases). For comparison we have also included the phase diagram for a value $\rho = 0.05 < \rho'$, with the χ_∞ line (solid) and the bifurcation line (broken).

boundary line separating the RM and DM regions. With further increase of $\rho > \rho'$ the new boundary line moves upwards to the right in the phase diagram, progressively reducing the DM region [Fig. 6(c)]. At a second special value (see Sec. IX)

$$\rho'' = \frac{J_1}{J_2}\frac{H_{A1}^*}{H_{A2}} = \frac{J_1}{J_2}\frac{1}{(1+2\xi+2\sqrt{\xi})}, \tag{9}$$

where $\xi = A_1 J_1 / A_2 J_2$, the region at infinite thickness of both phases ($t_1, t_2 \to \infty$) becomes RM, so that for $\rho > \rho''$ the DM region either disappears or becomes an island in the phase

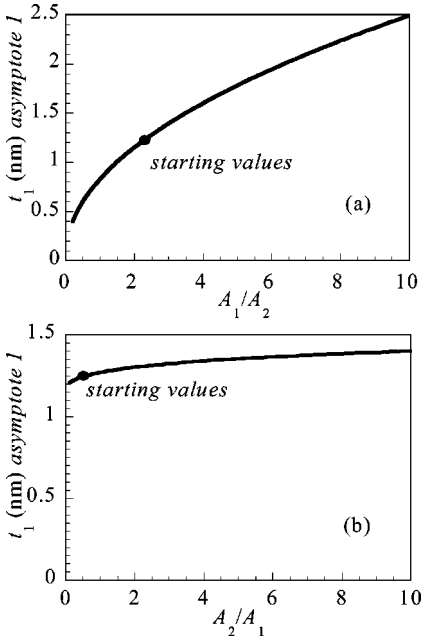

FIG. 7. Soft/Sm-Co composite system (starting data from Ref. 16): (a) soft-phase half-thickness position of first asymptote of the χ_∞ line as a function of the A_1/A_2 ratio, with A_2 fixed. (b) Soft-phase half-thickness position of first asymptote of the χ_∞ line as a function of the A_2/A_1 ratio, with A_1 fixed. The dots on the lines represent the starting values of A_1 and A_2 taken from Ref. 16.

diagram. The numerical values of ρ'' are 0.096 for soft/NdFeB and 0.148 for soft/Sm-Co.

The variation of the anisotropy ratio has little effect on the soft half-layer thickness position of the first asymptote, while strongly influences the position of second asymptote. This fact is summarized in Fig. 6(b), where the asymptote's positions in the phase diagram are reported as a function of K_1/K_2 ratio for the case of the soft/Sm-Co system. In the limit of vanishing soft phase anisotropy, the position t_1 of first asymptote tends to a value (1.23 nm), which is close to the exchange length $\delta_2 = \sqrt{A_2/K_2}$ of the hard Sm-Co phase (about 1.55 nm), while the position of the second asymptote tends to infinite thickness.

In the particular case $K_1 = 0$, $K_2 = K$, $A_1 = A_2 = A$, $J_1 = J_2$, the position of the first asymptote turns out to be $t_1\sqrt{K/A} = 0.985013$, in good agreement with the boundary thickness between the continuous and discontinuous jump of the magnetization at nucleation as reported by Aharoni[35] ($t_1\sqrt{K/A} = 0.984$). The positions of the two asymptotes collapse, as already stressed, for $K_1/K_2 = 0.06$, in correspondence to a soft half-layer thickness of 2.8 nm for the case of the soft/Sm-Co system [Fig. 6(b)].

We also analyzed how the position of the first asymptote is influenced by the variation of exchange constants. As a first attempt, we fixed K_1 and K_2 to the initial values of Ref. 16 and changed either A_1 or A_2. The results for the case of the soft/Sm-Co system are reported in Figs. 7(a) and 7(b), from which it can be inferred that A_1 determines the strongest variation of the asymptote position: about 70% for a change of a factor 10 of the A_1/A_2 ratio.

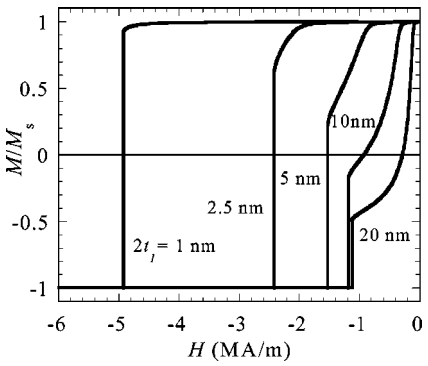

FIG. 8. Demagnetization curves for the case of a Fe/Sm-Co multilayer, with parameters $M_1=1.7$ MA/m, $M_2=0.55$ MA/m, $K_1=10^2$ J/m^3, $K_2=5$ MJ/m^3, $A_1=2.8\times10^{-11}$ J/m, $A_2=1.2\times10^{-11}$ J/m (data from Ref. 16). The hard-layer thickness ($2t_2$) is fixed at 20 nm and those of the soft layer ($2t_1$) are indicated (in nm) on the curves. The calculation was performed considering a tilting angle of 3° between the easy axis and the field direction, as in Ref. 16.

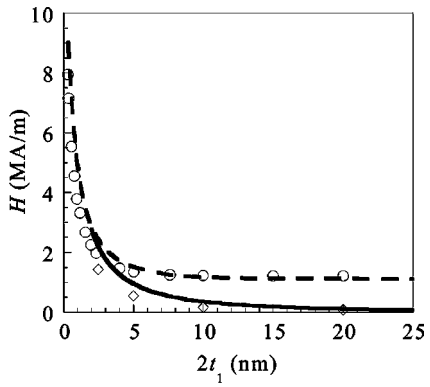

FIG. 9. Comparison between the calculated critical fields H_{c1} (continuous line) and H_{c2} (dashed line) and the corresponding values obtained in Ref. 16, as functions of the soft-layer thickness ($2t_1$), having fixed the hard-layer thickness at 20 nm. Open diamonds, H_{c1}; open dots, H_{c2}.

VII. THE CALCULATED DEMAGNETIZATION CURVES

The procedure for tracing by numerical calculations the demagnetization curves of an exchange-coupled multilayer is reported in Appendix C. Figure 8 reports the calculated demagnetization curves for a Fe/Sm-Co system, with the same intrinsic parameters utilized by Fullerton *et al.*[16] In this case the curves refer to the same Sm-Co layer thickness (20 nm) and different Fe layer thicknesses in the range 1–20 nm, as in Fig. 10(a) of Ref. 16. The calculation was performed considering a tilting angle of 3° between the easy axis and the field direction, as in Fullerton *et al.*[16] The comparison of calculated curves with those reported in the cited reference gives a good agreement concerning the shape and the H_{c1} and H_{c2} values down to a soft-layer thickness of about 5 nm, that is, for systems lying in the ES region. However, we observe an increasing discrepancy for the calculated H_{c2} value on reducing the $2t_1$ value below 5 nm.

The values of H_{c1} and H_{c2} as functions of the soft-layer thickness are reported in Fig. 9, together with the corresponding critical field values calculated in Fullerton *et al.*[16] There is good agreement for H_{c2}, especially at large thicknesses, while our H_{c1} values seem to be slightly larger than those obtained in Fullerton *et al.*[16] The transition to the RM regime appears in both calculations to occur at roughly the same thickness $2t_1\approx2$ nm. Amato *et al.*,[29] on the basis of a discrete micromagnetic model, calculated the demagnetization curves for the Fe/Sm-Co exchange-spring multilayer, utilizing the same data given by Fullerton *et al.*[16] The comparison of the results from our model and those of Amato *et al.*[29] is difficult because they consider a *finite* multilayer system, with constant total thickness and different nanostructuration degree, that is, different number of layers. Furthermore, because the systems of Amato *et al.*[29] start and finish with a hard layer, they show a symmetry that we cannot exactly reproduce: this is true in particular for the systems with a small number of layers. Nevertheless, we numerically calculated, on the basis of our model, the demagnetization curves for infinite multilayers having the same layer thicknesses of the finite systems considered by Amato *et al.*[29] The only exception is the case of trilayer ($n=3$) for which we have also calculated the curve considering the system as composed by two symmetrical bilayers having half thicknesses 10 nm/10 nm. These curves are reported in Fig. 10, to be compared with Fig. 2 of Ref. 29 and the deduced values of the critical fields H_{c1} and H_{c2} are compared in Table I with the corresponding values of Amato *et al.*[29] Our critical fields H_{c1} and H_{c2} are larger than those deduced by Amato *et al.*,[29] independently of the nanostructuration degree. Furthermore, our system enters the RM regime for smaller values of the nanostructuration degree of the multilayer. However, the general features of the demagnetization curves turn out to be similar. In general, from this comparative analysis we can say that the continuous micromagnetic approach gives reliable results down to layer thicknesses of a few atomic layers.

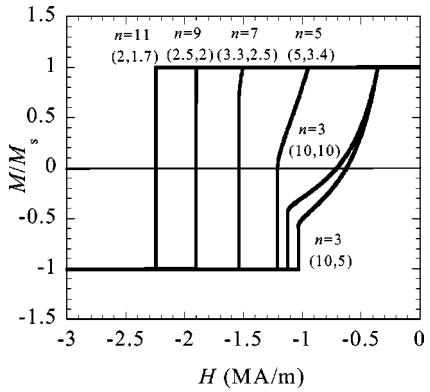

FIG. 10. Series of calculated demagnetization curves for infinite Fe/Sm-Co exchange-spring multilayer having the same layer-thicknesses of the finite systems of Ref. 29. The *n* value reported on the curves represents the nanodispersion index, as defined in Ref. 29, that is, $n=3$ corresponds to a trilayer, $n=5$ to a pentalayer, and so on. The numbers in parentheses represent the soft and hard half-layer thickness expressed in nm.

TABLE I. The calculated critical fields H_{c1} and H_{c2} compared with the corresponding values obtained in Ref. 29. The n value represents the nanodispersion index, as defined in Ref. 29, that is, $n=3$ corresponds to a trilayer, $n=5$ to a pentalayer, and so on. The soft and hard half-layer thickness is expressed in nm.

	Nanodispersion index					
	$n=11$	$n=9$	$n=7$	$n=5$	$n=3$	$n=3$
H	soft/hard layer thickness					
(MA/m)	2/1.7	2.5/2	3.3/2.5	5/3.4	10/10	10/5
H_{c1}[a]	1.79	1.42	0.99	0.60	0.21	0.21
H_{c1}[b]	2.24	1.90	1.49	0.93	0.36	0.36
H_{c2}[a]	1.77	1.54	1.31	1.18	1.07	1.07
H_{c2}[b]	2.24	1.90	1.54	1.21	1.13	1.04

[a]Ref. 27.
[b]This work.

VIII. COMPARISON WITH EXPERIMENTAL DATA

The magnetic behavior of a planar magnetic nanocomposite described in the previous paragraphs, in particular the demagnetization processes, can in principle be conveniently compared with experimental results on real systems. Among the observed phenomena we believe that the nucleation at the critical field H_{c1} in the ES region is properly described by the present model because the system undergoes a second-order transition to a reversible state, so that it is in a favorable condition to be insensitive to localized defects or inhomogeneities.[50] These are instead known to be of major importance in the coercivity mechanisms involving an irreversible transition (Brown paradox). As a matter of fact the values of the H_{c2} field that the model predicts are based on a condition of instability of inhomogeneous rotation processes and are strictly valid for a perfectly homogeneous system. In other words our model does not include inverse domain nucleation and propagation, at least for the case of a proper exchange-coupled system, i.e., in the ES and RM states. As a consequence the obtained H_{c2} values are to be intended as an upper limit for the real reversal field, in a way similar to the switching field in the Stoner-Wohlfarth model.

We made an attempt to compare the hysteresis cycles of the $Ni_{80}Fe_{20}/Sm_{40}Fe_{60}$ system reported in Ref. 11 with those deduced from our model, on the basis of the following material parameters: the saturation magnetization of both phases ($M_1=860$ kA/m, $M_2=286$ kA/m, from Ref. 12) and the anisotropy constant (assumed to be zero) of $Ni_{80}Fe_{20}$. The other quantities (exchange constants of both phases and anisotropy constant of the hard phase) were considered as free parameters in a best-fit procedure concerning the soft- and hard-layer thickness dependence of H_{c1}, as deduced from Figs. 3 and 4 of Ref. 11. The results of the best fit are shown in Figs. 11(a) and 11(b), corresponding to a given $2t_1$ value (57.6 nm) and to a given $2t_2$ value (100 nm), respectively. The obtained values of the free parameters are $K_2=2.2\times10^4$ J/m^3 and $A_1=A_2=6.5\times10^{-12}$ J/m.

For the above explained reasons, it has to be underlined that we only took into account the experimental hysteresis cycles that manifestly are in the ES regime and for which we identify the nucleation field with the critical field H_{c1} of our model. In these cycles it turns out that the reversal occurs at fields substantially lower than the theoretical H_{c2} values [Figs. 11(a) and 11(b)]. It is worth noting that this discrepancy is progressively reduced on increasing both layer thicknesses, i.e., approaching the DM regime [see Fig. 11(b)]. With $2t_1>60$ nm and $2t_2=100$ nm we have a substantial agreement between experimental and theoretical values of H_{c2}, which appear to be independent of the soft-layer thickness. This limit of H_{c2} corresponds amazingly to the domain wall depinning field at the hard-soft interface as described in the next section.

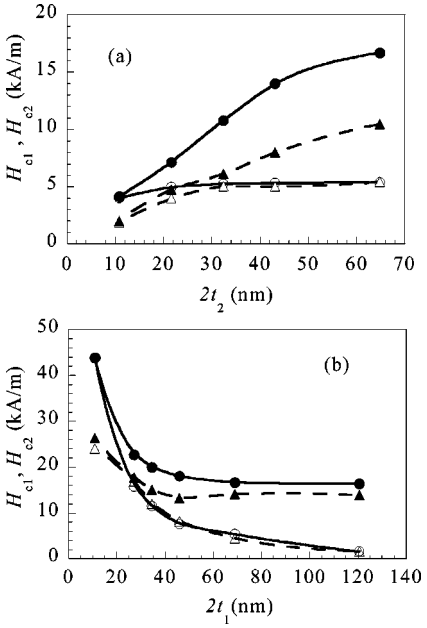

FIG. 11. Comparison between calculated and experimental (from Ref. 11) critical fields H_{c1} and H_{c2} for a series of exchange-spring bilayers and trilayers based on the $Ni_{80}Fe_{20}/Sm_{40}Fe_{60}$ system: (a) in the case of a fixed soft-layer thickness $2t_1=57.6$ nm, (b) in the case of a fixed hard-layer thickness $2t_2=100$ nm. The open symbols refer to H_{c1}, while the filled symbols to H_{c2}; triangles refer to data taken from Ref. 11 and circles refer to our calculations. The material parameters were considered as free parameters in a best-fit procedure, with the exception of the saturation magnetization of both layers and the anisotropy constant of $Ni_{80}Fe_{20}$, assumed to be zero. The obtained values of the free parameters are $K_2=2.2\times10^4$ J/m^3 and $A_1=A_2=6.5\times10^{-12}$ J/m. The lines are guides for the eyes.

An example of demagnetization curves for different soft-layer thicknesses, calculated by using the obtained material parameters, is shown in Fig. 12, where the hard-layer thickness is fixed at 100 nm. They are in qualitative agreement with the experimental curves particularly on the reversible portion where there is a slight difference in the average slope. Moreover Fig. 13 reports the phase diagram of the $Ni_{80}Fe_{20}/Sm_{40}Fe_{60}$ system obtained from our theory, with the critical line χ_∞, which is compared with the critical line reported in Fig. 7 of Ref. 11, defining the transition from single-switching process to exchange-spring process. It is evident that there is a pronounced discrepancy between the

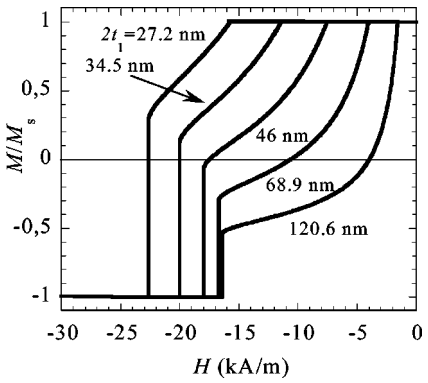

FIG. 12. Series of calculated demagnetization curves of $Ni_{80}Fe_{20}/Sm_{40}Fe_{60}$ multilayers (data from Ref. 11) in the ES regime, in the case of a fixed hard-layer thickness $2t_2=100$ nm for different soft-layer thicknesses $2t_1$.

two curves, particularly in the low soft-layer thickness region. We explain this difference by admitting that in general for the experimental hysteresis loops (Fig. 4 of Ref. 11) exhibiting a single switching the reversal occurs before the system could reach the instability condition at the nucleation field. This irreversible switching could be ascribed to an inhomogeneous reversal caused by extrinsic factors, while our model gives, as an upper limit, an irreversible switching field H_{c2} only based on rotation processes. Domain observations have been indeed recently performed on $Ni_{80}Fe_{20}/Sm_{40}Fe_{60}$ exchange-spring films using Kerr microscopy in applied magnetic fields.[51] On the other hand the critical curve reported in Fig. 7 of Ref. 11 can be considered at most as an empirical fitting curve of the experimental results. As a matter of fact the theoretical interpretation given in Ref. 11 is inconsistent because it is based on an inverse power law [Eq. (1)] with exponent 1.75. The point is that this power dependence, as explained in Ref. 27, does not refer to the conventional definition of the nucleation field given in micromagnetism, but rather to the irreversible switching field,

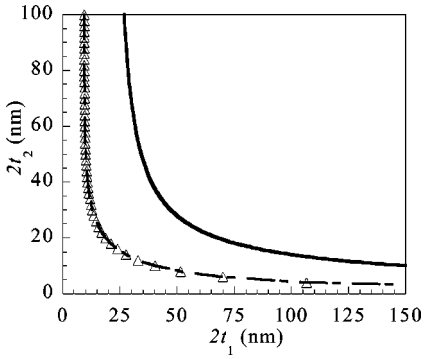

FIG. 13. Phase diagram of the $Ni_{80}Fe_{20}/Sm_{40}Fe_{60}$ system (data from Ref. 11), with the critical line χ_∞ (triangles and dash-dotted line) compared with the critical line (solid line) for the transition from single-switching process to exchange-spring process, as reported in Fig. 7 of Ref. 11. The material parameters utilized to trace the phase diagram were deduced from a best-fit procedure (see Fig. 11).

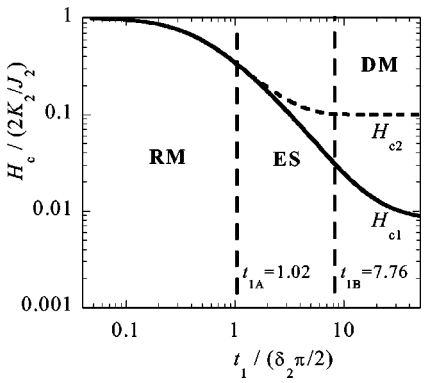

FIG. 14. Fe/NdFeB composite system (data from Ref. 27): soft half-layer thickness dependence of critical fields H_{c1} and H_{c2}, in the case of a thick hard layer ($t_2=100$ nm). The critical fields are normalized to the hard-layer anisotropy field, while t_1 is normalized to the hard-layer DW half width $(\pi/2)\delta_2$. The vertical dashed lines represent the boundaries of different regions in the magnetic phase diagram (see Fig. 3).

according to the meaning given to the term ''nucleation'' in Ref. 27 (see also next section).

IX. THE LIMIT OF A HARD BULK WITH A SOFT PLANAR INCLUSION

As outlined in Sec. III, the problem of reduction of the nucleation field in a hard bulk containing a soft planar inclusion was first discussed by Aharoni and, later, Abraham on the basis of a micromagnetic one-dimensional model,[35,37] which is rather similar to that adopted by Leineweber *et al.*[27] for the hard-soft exchange-coupled triple layer (where the infinite extension of the hard layers makes the system a hard bulk). Moreover, the same model was also utilized by Goto *et al.*[25] with the only difference that the soft layer is considered coupled to a hard bulk only on one side. In principle, the results of all these models should be obtained from our model in the limit case of a very thick (ideally infinite) hard layer. Note that both Aharoni[35] and Goto *et al.*[25] assumed a zero-anisotropy soft layer.

As already outlined in Sec. V, for large hard-layer thicknesses the phase diagram appears to be subdivided into three regions by the vertical asymptotes of the critical line χ_∞: the hard-dominated RM region, the ES region, and the soft-dominated DM region. We report in Fig. 14 the soft-layer thickness dependence of the critical fields H_{c1} and H_{c2} in the case of a Fe/NdFeB composite, having set a large value of the hard-layer thickness ($t_2=100$ nm). The two vertical asymptotes correspond in this case to $t_1=t_{1A}=2.15$ nm $\approx(\pi/2)\delta_2$, where $\pi\delta_2$ represents the hard-layer Bloch wall width, and $t_1=t_{1B}=16.3$ nm: the asymptote positions are indicated in Fig. 14 by dashed lines. Inside the RM region the critical fields coincide, as expected, and the character of H_{c1} in the DM region is modified with respect to the ES region, because it represents here a true reversal field for the soft layer, that is, the starting of an irreversible process.

For the case of a NdFeB/Fe/NdFeB trilayer, Leineweber

et al. calculated the soft-layer thickness dependence of the field at which the irreversible inversion occurs (Fig. 4 of Ref. 27). Our analysis shows the following (see Fig. 14). (i) For $t_1 < (\pi/2)\delta_2$, the nucleation field H_{c1} is rather different from the anisotropy field of the hard layer $H_{A2} = 2K_2/J_2$, except that H_{c1} reaches the value of H_{A2} only when $t_1 \to 0$. (ii) It is reduced by a factor 3 when $t_1 = t_{1A}$. This means that even a very thin soft layer coating on a hard bulk dramatically reduces the nucleation (or reversal) field in the RM regime. (iii) The nucleation field H_{c1} asymptotically tends to the value of the soft-layer anisotropy field $H_{A1} = 2K_1/J_1$, as expected. These results are in contradiction to the behavior shown in Fig. 4 of Ref. 27, where the reversal field is constant for $t_1 < (\pi/2)\delta_2$, while for $t_1 > 10(\pi/2)\delta_2$ we cannot observe neither for H_{c1} nor for H_{c2} the inverse power-law behavior $\propto (t_1)^{-1.75}$, as reported in Ref. 27.

The limit of H_{c2} for $t_1 \to \infty$ corresponds to the domain-wall depinning field at the hard-soft interface,[52] which is an important coercivity mechanism in the case of a hard bulk enclosing a soft inclusion. In bulk permanent magnets, the depinning of a domain wall may be the rate limiting step of flux reversal, thus representing a more realistic mechanism as compared to intrinsic nucleation (characterized by the anisotropy field).[53] Nucleation centers exist indeed on surfaces and along hard-soft grain boundaries (in the very common case of presence of soft phase inclusions), which obviate the onset of the intrinsic process.

In this particular case it is possible to obtain an analytical expression of the reversal field H_{c2}. To this purpose we assume both t_1 and $t_2 \to \infty$, a situation corresponding to a hard bulk exchange-coupled to a soft bulk at the interface. We are in general in the case of a system in the DM regime (except when K_1/K_2 is above a certain value, as explained in Sec. VI), and we are considering the intermediate state after the reversal of the soft phase, so that we assume $\vartheta_1 = \pi$ and $\vartheta_2 = 0$. The system of equations is given by Eq. (3) plus Eq. (A7). From this an equation in H and ϑ_0 is obtained:

$$F(H,\vartheta_0) = [A_2J_2(\cos\vartheta_0 - 1) - A_1J_1(\cos\vartheta_0 - \cos\vartheta_1)]H - (A_1K_1 - A_2K_2)\sin^2\vartheta_0 + A_1K_1\sin^2\vartheta_1 = 0. \tag{10}$$

The condition for H_{c2} is $dH/d\vartheta_0 = 0$ that implies $\partial F(H,\vartheta_0)/\partial\vartheta_0 = 0$. Elimination of ϑ_0 between the latter equation and Eq. (10) allows one to obtain the following equation for H:

$$(A_2J_2 - A_1J_1)^2H^2 - 4(A_2K_2 - A_1K_1)(A_2J_2 + A_1J_1)H + 4(A_2K_2 - A_1K_1)^2 = 0. \tag{11}$$

The only solution having physical meaning is the lower one. It provides the analytical expression of the domain-wall depinning field H_{DW} (Ref. 52):

TABLE II. The calculated domain wall depinning field H_{DW} for different hard-soft composites. The intrinsic magnetic parameters are taken from Refs. 16 and 27. Co-soft represents an extremely fine-grained Co with anisotropy constant reduced by a factor 10^3.

composite	H_{DW} (MA/m)	H_{A2} (MA/m)	H_{DW}/H_{A2} (%)
Fe/NdFeB[a]	0.540	5.347	10.10
Co/NdFeB[a,b]	0.669	5.347	12.52
Fe/Sm-Co[b]	2.011	14.469	13.90
Co-soft/Sm-Co[b]	3.021	14.469	20.88
Co/Sm-Co[b]	2.859	14.469	19.76

[a]Parameters taken from Ref. 27.
[b]Parameters taken from Ref. 16.

$$H_{DW} = 2\frac{A_2K_2 - A_1K_1}{A_2J_2 + A_1J_1 + 2\sqrt{A_1A_2J_1J_2}}. \tag{12}$$

In the case of a Fe/NdFeB system, Eq. (12) gives $H_{DW} = 0.543$ MA/m, which is about 10% of the hard-phase anisotropy field H_{A2}. Table II reports the calculated DW depinning field H_{DW} for different hard-soft composites: it is worth noting that the obtained values are in all cases of the order of 10–20% with respect to the hard-phase anisotropy field.

The reversal field calculated by Aharoni in Ref. 35 (therein termed "coercive force") for the case $K_1 = 0$, $K_2 = K$, $A_1 = A_2 = A$, $J_1 = J_2$, as already mentioned in Sec. VI, can be considered as a particular case of Eq. (12), which gives $H_{DW} = 0.25H_{A2}$, in agreement with the value reported in Ref. 35. It should be emphasized that the periodic boundary conditions at the basis of the present treatment are consistent with the boundary conditions assumed in the abovementioned work.

To summarize, we were not able to reproduce the results of the analysis of Leineweber *et al.* as a limit of our model for very large t_2 values. Nevertheless, the results reproduced in Fig. 14 compare well with those of Fig. 1 of Ref. 35, where the nucleation field and the coercive (reversal) field are reported as functions of the soft-layer size in reduced units. The agreement is even better for very thin soft layers.

There is however, in principle, a possible physical situation that is not included in the abovementioned periodic boundary conditions for the composite multilayer. As we have seen these conditions imply a reversal mechanism involving the whole system in a cooperative rotation process: the displacement of a domain wall is *a priori* excluded for a RM and an ES state, while a DW depinning process at the hard-soft interface occurs in the case of DM phase. A different situation can in principle be envisaged by assuming antiparallel domains at infinity as a boundary condition: in this case the periodicity of the system is in fact lost. The study of the multilayer under these new circumstances could throw new light on the coercivity mechanism of the domain wall pinning. A similar situation was considered in the treatment of Friedberg and Paul[54] concerning domain wall pinning process in a bulk uniaxial magnet, having a planar soft inclu-

sion, to be compared with the classical nucleation mechanism in the bulk.[35] In the case of a composite multilayer, this condition of antiparallel domains should correspond to consider the propagation of a domain wall throughout the system and eventually to observe an intrinsic type of coercivity, due to the matching between the DW width and the layer thicknesses. The analogy is with the proper ''intrinsic coercivity'' connected with the DW pinning in a homogeneous magnetic crystal having very high anisotropy and thus narrow domain walls. The intrinsic coercivity originates from the modulation of the DW energy by the lattice periodicity.[55]

Having introduced the depinning field we can reconsider here the modifications of the magnetic phase diagram on varying the anisotropy ratio ρ, as explained in Sec. VI. In particular, there is a critical value $\rho=\rho''$ for which the DM phase disappears at infinite thickness of both phases [see Eq. (9)]. In order to obtain this critical value the condition is that the depinning field equals the critical field H_{c1}, which in this limit coincides with the soft phase anisotropy field. Hence we have the equation

$$2\frac{A_2K_2-A_1K_1}{A_2J_2+A_1J_1+2\sqrt{A_1A_2J_1J_2}}=\frac{2K_1}{J_1} \tag{13}$$

which yields

$$\frac{H_{A1}}{H_{A2}}=\frac{1}{(1+2\xi+2\sqrt{\xi})}, \tag{14}$$

where $\xi=A_1J_1/A_2J_2$. Expression (14) provides the critical value ρ'' given by Eq. (9).

As a final remark we have verified the agreement of our model with the one of Goto *et al.*[25] In that model the exchange-bias field, which corresponds to the nucleation field H_{c1} of our treatment, results to be inversely proportional to the squared soft-layer thickness. In order to compare the two models, we fixed the soft-layer anisotropy to a very low value (10^{-6}), while the hard-layer anisotropy was chosen equal to that of Sm-Co in Ref. 10. Furthermore, the thickness ratio t_2/t_1 was kept equal to 10^3. We obtained a perfect agreement between the results of our treatment in this limit and the power law predicted by the model of Goto *et al.*, concerning the soft-layer thickness dependence of H_{c1}.

X. THE MAXIMUM ENERGY PRODUCT

Although the exchange-spring shows such an interesting reversibility property it is not perhaps the best condition to achieve the maximum energy density, which is a prerequisite for a high-performance permanent magnet. It is likely that the best composite permanent magnet should be realized in the RM state because the magnetization remains at its maximum value in the presence of a reverse field.

A. Optimum $(BH)_{max}$: a convenient criterion

The analysis of the phase diagram for the Fe/Sm-Co multilayer (Fig. 2) allows us to deduce that an RM system with significant technical parameters is expected for layer thicknesses of about 8 and 3 nm, for the soft and hard components respectively.[44] In this case, H_{c1} would be of the order of 1 MA/m, while the average remanent magnetization

$$M_r=(M_1t_1+M_2t_2)/(t_1+t_2) \tag{15}$$

turns out to be close to 1.4 MA/m, with a corresponding $(BH)_{max}$ of about 0.6 MJ/m^3.

In general, if we are interested in obtaining a multilayer with the largest possible layer thicknesses in the RM region, then an optimum point in the phase diagram should exist for the maximum energy product. This point must be on the χ_∞ critical line and is determined from the condition $H_{c1}=M_r/2$. As an example we have utilized the phase diagram calculated for the Fe/NdFeB system (Fig. 3) to obtain the optimum point corresponding to $(BH)_{max}$: the deduced values are $t_1=4.4$ nm, $t_2=1.8$ nm, $H_{c1}=0.8$ MA/m, and $(BH)_{max}=0.8$ MJ/m^3. For real samples, one has to consider the influence of extrinsic factors on the coercive behavior, such as, the imperfect moment orientation of the hard layers, which could reduce considerably the coercive field with respect to the critical field H_{c1}, and then the energy product (see below).

B. The limit of extreme nanostructuration

A further possibility offered by the phase diagram is to analyze the region of very thin layers, in the neighborhood of the origin, corresponding to the limit of small t_1 and t_2, as compared to $(\alpha_1/2)^{-1/2}$ and $(\beta_2)^{-1/2}$, respectively (see Sec. IV). In such conditions the magnetic moments rotation is almost uniform and H_{c1} approaches the value of an effective anisotropy field

$$\overline{H_A}=2(K_1t_1+K_2t_2)/\mu_0(M_1t_1+M_2t_2), \tag{16}$$

that is the weighted average of the anisotropy fields of the two phases. This condition is equivalent to an extreme nanostructuration of the multilayer, which, in principle, could allow us to achieve very high-energy products.[16,29] In this case, it could be of interest to evaluate the soft-phase volume fraction $\lambda=t_1/(t_1+t_2)$ for an optimum $(BH)_{max}$, in correspondence to a given hard material. To define the ''optimum'' energy product, we refer again to the criterion $H_{c1}=H_{c1}^*=M_r/2$, in this case with $H_{c1}\approx\overline{H_A}$. By substituting the above conditions in Eq. (15) we obtain an equation in λ (Ref. 44):

$$(M_1-M_2)^2\lambda^2+2\left[M_2(M_1-M_2)+2\left(\frac{K_2}{\mu_0}-\frac{K_1}{\mu_0}\right)\right]\lambda+M_2^2-4\frac{K_2}{\mu_0}=0. \tag{17}$$

If we assume a negligible anisotropy for the soft phase, i.e., $K_1=0$, and that the hard-phase anisotropy constant K_2 is

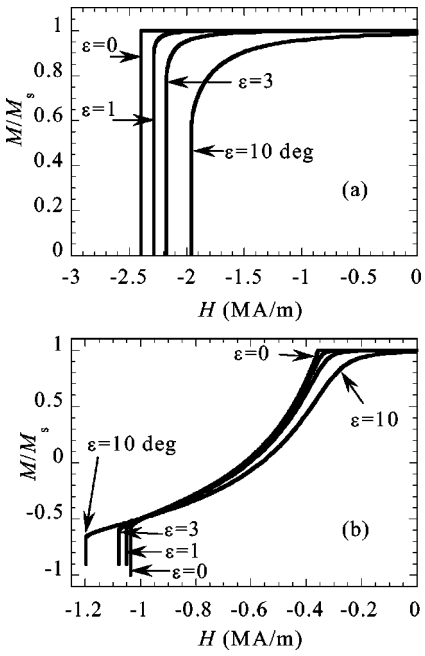

FIG. 15. Series of calculated demagnetization curves for the case of a Fe/Sm-Co multilayer, with the material parameters reported in Ref. 16, with different angles ε (deg.) between the magnetic field direction and the easy-axis direction: (a) in the case $t_1 = t_2 = 2$ nm (RM region); (b) in the case $t_1 = 10$ nm and $t_2 = 5$ nm (ES region).

very large with respect to $\mu_0 M_1^2$, the solution of Eq. (17) simply reduces to $\lambda \approx 1 - \mu_0 M_1^2 / 4K_2$. It turns out that the soft phase volume ratio is independent of the hard-phase magnetization. In other words, for a very hard phase, λ approaches unity and the relevance of M_2 in the overall magnetization is accordingly reduced. Therefore, in the case of extreme nanostructuration, it would be possible in principle to utilize hard phases having low or virtually zero magnetization, i.e., ferrimagnets or even antiferromagnets, to build a planar nanocomposite magnet with the optimum energy product. In this case, one might think to exploit the very large crystal anisotropy of intermetallic phases such as the heavy rare-earth–transition metal ($TbCo_5$) or the Laves phases. This principle has recently found practical realization in the anti-ferromagnetically coupled $DyFe_2$-YFe_2 superlattices,[56] grown by molecular beam epitaxy. Moreover the high degree of nanostructuration implies a large surface to volume ratio that makes surface or interface anisotropy a further element to come into play.

C. Effect of misalignment

As a further aspect, the orientation of the hard phase has an important role in the overall performance of real magnets. From this viewpoint, we have analyzed the effect of the existence of a nonzero angle ε (deg.) between the soft- and hard-layer easy axis and the field direction. This situation resembles that of a real system, in which a distribution of the hard-layer easy axis orientations is likely to be realized. We have observed two distinct behaviors of the systems in the RM and ES regime. If we consider a multilayer with material parameters as in Ref. 16, the reversal field H_{c2} decreases with increasing the angle ε if the system belongs to the RM regime [Fig. 15(a)], while the opposite occurs for the ES regime [Fig. 15(b)]. The singularity associated with the nucleation field H_{c1} is only present for a perfect alignment, i.e., $\varepsilon = 0°$. A finite angle ε, whatever small, actually rules out the singularity and the kink point is progressively rounded off. It is a case of a broken symmetry and actually all the magnetic moments start to rotate immediately after the application of an infinitesimal field. Figure 16 shows the effect of a small misorientation on the critical field H_{c2}, in the case of systems in the RM and ES regimes.

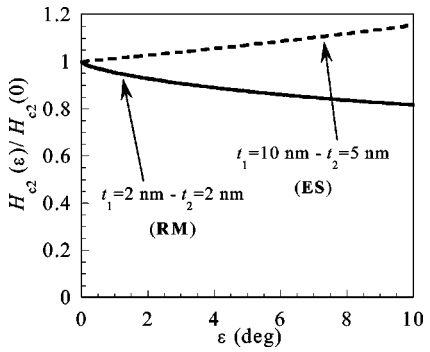

FIG. 16. Critical field H_{c2} as a function of the misorientation angle ε (deg.) between the magnetic field direction and the easy-axis direction for the case of a Fe/Sm-Co multilayer. The two lines correspond to the cases considered in Fig. 15. The H_{c2} values are normalized to that corresponding to $\varepsilon = 0°$.

XI. CONCLUSIONS

The magnetic composite can present peculiar magnetic properties that are absent in homogeneous phases, in particular depending on the microstructural parameters. In fact there is the need of a basic phenomenological description of a physical system of this kind. A magnetic phase diagram in terms of important microstructural parameters such as the layer thicknesses, in the case of a planar composite, is a first step in this direction. We have developed a one-dimensional micromagnetic model of the multilayer exchange-spring magnet, which leads to a complete magnetic phase diagram for the planar hard-soft nanocomposite, providing a powerful tool for a general overview of its magnetic properties. In particular it gives information on the type of demagnetization processes and the critical fields at which nucleation and reversal take place. The diagram has in principle a predictive potential on the behavior of particular configurations and therefore is useful for the tailoring of these artificial materials.

A key point to this purpose is the analytical expression we have obtained in Eq. (8) for the critical susceptibility at the nucleation field. Depending on the sign of this quantity, we have a reversible or an irreversible switching, corresponding respectively to the exchange-spring magnet (ES) or to the rigid composite magnet (RM) regime, for very small soft-

layer thicknesses. On the side of large soft-layer thicknesses we find again a negative value of the critical susceptibility, but it corresponds now to the condition of decoupled magnet (DM), in which the irreversible switching occurs in two steps, i.e., almost independently in the two phases. The boundary line between the different regimes is an U-shaped line corresponding to divergence of the critical susceptibility. Then for large values of the soft-layer thickness the system goes directly from RM to DM phase on increasing the hard-layer thickness, without crossing the ES region. The diagram also reports the iso-critical lines both for the nucleation and the reversal field. These lines bifurcate along the RM boundary line.

Noticeably, for a given hard material the ES phase is predicted to occur only below a threshold of the ratio between the anisotropy constants of the two phases K_1/K_2. For example, the threshold is of the order of a few % for the case of Sm-Co and NdFeB hard phases. Well above this limit, but remarkably still far from unity, it happens that even the DM disappears.

The limit of infinite hard-layer thickness gives information on the behavior of bulk magnets with planar soft inclusions. It is worth noting that even a soft layer as thin as the hard-phase Bloch wall is enough to cause a fall of the nucleation field to 1/3 of the hard-phase anisotropy field. The limit of both infinite hard-and soft-layer thicknesses provides the analytical expression of the critical field pertinent to an important coercivity mechanism of permanent magnets: the domain-wall depinning.

In general, the adopted model is limited to rotational processes: in fact, the deduced values of the reversal fields are systematically larger than the experimental ones. This is clearly due to the fact that the model does not consider the role of domains and DW nucleation and pinning,[57] except in the abovementioned case of the decoupled system. Hence the obtained values of the reversal field should be considered as an upper limit, in analogy with the switching field of the Stoner-Wohlfarth model with respect to the coercivity of real bulk magnets. Moreover, because of the chosen one-dimensional ansatz, we exclude *a priori* the possible role of topological singularities.[57]

Another intrinsic limitation of our model is that it is based on the continuum approximation. However, the comparison with the results of discrete one-dimensional models reported in the literature shows that the micromagnetic approach is a good representation of the real system, down to thickness of a few atomic layers.

A characteristic, which is common to our model and to practically all the other treatments reported in the literature and discussed in the present work, is the assumption of the magnetization lying in the film plane. However we have also considered the implications of admitting a perpendicular anisotropy and we have given some indications how to apply our analysis to this case.

Furthermore, we have addressed the problem of the technical performance of a planar composite permanent magnet. The maximum energy density requires the magnetization to be as high as possible, so that best performance is expected in the RM state. If one wants to conveniently utilize the largest layer thicknesses, the optimum $(BH)_{\max}$ should be searched along the RM-ES boundary line. On the other hand it turns out that, in the limit of vanishing layer thicknesses and of very large hard-phase anisotropy, an even higher $(BH)_{\max}$ is achievable for an optimum soft-phase volume fraction (close to unity) depending only on the soft phase magnetization. This means that it is possible in principle to employ hard phases having low or virtually zero magnetization, i.e., ferrimagnets or even antiferromagnets.

The orientation of the hard phase has an important role in the overall performance of real systems. We have analyzed the effect of a small misalignment of the easy axis and observed that the reversal field decreases with increasing the misorientation angle if the system belongs to the RM regime, while the opposite occurs for the ES regime.

The planar nanocomposite magnets have in perspective other reasons of interests, such as the role of the microstructure (multilayers vs hard-granular layered systems), the DW pinning process, and the rediscovery of the intrinsic DW pinning on a mesoscopic scale, by matching microstructure length scale with domain wall width.

ACKNOWLEDGMENTS

The present work has been supported by a FIRB Project of the Italian Ministry of Education and Research, entitled ''Microsystems based on magnetic materials structured on a nanoscopic scale.''

APPENDIX A: FOURTH-ORDER EXPANSION

We start from Eq. (4), which is the power expansion up to the fourth order of Eq. (3). After integration between the extrema $(\vartheta_1, \vartheta_0)$ for the soft layer and $(\vartheta_0, \vartheta_2)$ for the hard layer we obtain

$$\vartheta_0 - \frac{p_1}{4}\frac{1}{\left(1+\frac{3}{4}p_1\vartheta_1^2\right)}\vartheta_0(\vartheta_1^2-\vartheta_0^2) = \vartheta_1\cos\left[\frac{(x_0-x_1)}{\left(1+\frac{3}{4}p_1\vartheta_1^2\right)}\sqrt{\frac{\alpha_1}{2}-\beta_1}\right], \tag{A1}$$

$$\vartheta_0 + \frac{p_2}{4}\frac{1}{\left(1+\frac{3}{4}p_2\vartheta_2^2\right)}\vartheta_0(\vartheta_0^2-\vartheta_2^2) = \vartheta_2\cosh\left[\frac{(x_0-x_2)}{\left(1+\frac{3}{4}p_2\vartheta_2^2\right)}\sqrt{\beta_2-\frac{\alpha_2}{2}}\right]. \tag{A2}$$

We perform now the substitutions $\vartheta_j \rightarrow \vartheta_j + \eta_j$ $(j=0,1,2)$, where the η_j are higher order infinitesimal quantities, and neglect in the calculations the terms of order higher than ϑ^3,

such as, $\eta\vartheta^2$ or $\eta^2\vartheta$. Then, we obtain two linear equations in the variables η_j, which are, in the case of the soft layer,

$$\eta_0-\eta_1\cos\left[(x_0-x_1)\sqrt{\frac{\alpha_1}{2}-\beta_1}\right]$$

$$=-\vartheta_0+\frac{p_1}{4}\vartheta_0(\vartheta_1^2-\vartheta_0^2)+\vartheta_1\left\{\cos\left[(x_0-x_1)\times\sqrt{\frac{\alpha_1}{2}-\beta_1}\right]+\vartheta_1^2(x_0-x_1)\frac{3p_1}{4}\sqrt{\frac{\alpha_1}{2}-\beta_1}\times\sin\left[(x_0-x_1)\sqrt{\frac{\alpha_1}{2}-\beta_1}\right]\right\} \quad \text{(A3)}$$

and for the hard layer

$$\eta_0-\eta_2\cosh\left[(x_0-x_2)\sqrt{\beta_2-\frac{\alpha_2}{2}}\right]$$

$$=-\vartheta_0+\frac{p_2}{4}\vartheta_0(\vartheta_0^2-\vartheta_2^2)+\vartheta_2\times\left\{\cosh\left[(x_0-x_2)\sqrt{\beta_2-\frac{\alpha_2}{2}}\right]-\vartheta_2^2(x_0-x_2)\times\frac{3p_2}{4}\sqrt{\beta_2-\frac{\alpha_2}{2}}\sinh\left[(x_0-x_2)\sqrt{\beta_2-\frac{\alpha_2}{2}}\right]\right\}. \quad \text{(A4)}$$

The next step consists of substituting, in the above equations, the reduced variables α_i $(i=1,2)$, which are related to the applied field H, with their expression in terms of the infinitesimal field τ. $\alpha_i\rightarrow\alpha_{i\mathrm{cr}}(1+\tau)$, where $\alpha_{i\mathrm{cr}}$ is the value of α_i at $H=H_{c1}$. Furthermore, we introduce the variables $\gamma_{1\mathrm{cr}}=\sqrt{\alpha_{1\mathrm{cr}}/2-\beta_1}$ and $\gamma_{2\mathrm{cr}}=\sqrt{\beta_2-\alpha_{2\mathrm{cr}}/2}$. Similarly, the critical variables $p_{i\mathrm{cr}}$ correspond to the expressions for p_i with $\alpha_i=\alpha_{i\mathrm{cr}}$. As a consequence of these substitutions and neglecting higher order terms, we transform Eqs. (A3) and (A4) in

$$\eta_0-\eta_1\cos[(x_0-x_1)\gamma_{1\mathrm{cr}}]$$

$$=-\vartheta_1\tau(x_0-x_1)\frac{\alpha_{1\mathrm{cr}}}{4\gamma_{1\mathrm{cr}}}\sin[(x_0-x_1)\gamma_{1\mathrm{cr}}]+\vartheta_1^3\gamma_{1\mathrm{cr}}\times(x_0-x_1)\frac{3p_{1\mathrm{cr}}}{4}\sin[(x_0-x_1)\gamma_{1\mathrm{cr}}]+\frac{p_{1\mathrm{cr}}}{4}\vartheta_0(\vartheta_1^2-\vartheta_0^2) \quad \text{(A5)}$$

for the soft layer and

$$\eta_0-\eta_2\cosh[(x_0-x_2)\gamma_{2\mathrm{cr}}]$$

$$=-\vartheta_2\tau(x_0-x_2)\frac{\alpha_{2\mathrm{cr}}}{4\gamma_{2\mathrm{cr}}}\sinh[(x_0-x_2)\gamma_{2\mathrm{cr}}]-\vartheta_2^3\gamma_{2\mathrm{cr}}(x_0-x_2)\frac{3p_{2\mathrm{cr}}}{4}\sinh[(x_0-x_2)\gamma_{2\mathrm{cr}}]-\frac{p_{2\mathrm{cr}}}{4}\vartheta_0(\vartheta_0^2-\vartheta_2^2) \quad \text{(A6)}$$

for the hard layer. A third equation is obtained by considering the boundary condition at $x=x_0$, which corresponds to the equilibrium condition for the exchange forces

$$\left(A_1\left.\frac{d\vartheta}{dx}\right|_{x=x_0-}=\right)A_1\sqrt{\alpha_1(\cos\vartheta_0-\cos\vartheta_1)+\beta_1(\sin^2\vartheta_0-\sin^2\vartheta_1)}$$

$$=\left(A_2\left.\frac{d\vartheta}{dx}\right|_{x=x_0+}=\right)A_2\sqrt{\alpha_2(\cos\vartheta_0-\cos\vartheta_2)+\beta_2(\sin^2\vartheta_0-\sin^2\vartheta_2)}. \quad \text{(A7)}$$

By performing the substitutions $\vartheta_j\rightarrow\vartheta_j+\eta_j$ $(j=0,1,2)$, and $\alpha_i\rightarrow\alpha_{i\mathrm{cr}}(1+\tau)$ $(i=1,2)$, and considering that the expansion of Eq. (A7) truncated to the second order gives the additional condition

$$A_1^2(\vartheta_1^2-\vartheta_0^2)\gamma_1^2=-A_2^2(\vartheta_2^2-\vartheta_0^2)\gamma_2^2, \quad \text{(A8)}$$

we obtain finally a system of three linear equations in the angles η_j:

$$\eta_0-\eta_1\cos[(x_0-x_1)\gamma_{1\mathrm{cr}}]$$

$$=(x_0-x_1)\gamma_{1\mathrm{cr}}\sin[(x_0-x_1)\gamma_{1\mathrm{cr}}]\times\left[-\frac{\tau\alpha_{1\mathrm{cr}}\vartheta_1}{2(\alpha_{1\mathrm{cr}}-2\beta_1)}+\frac{3p_{1\mathrm{cr}}}{4}\vartheta_1^3\right]+\frac{p_{1\mathrm{cr}}}{4}\vartheta_0(\vartheta_1^2-\vartheta_0^2),$$

$$\eta_0 - \eta_2 \cosh[(x_0-x_2)\gamma_{2cr}] = (x_2-x_0)\gamma_{2cr}\sinh[(x_0-x_2)\gamma_{2cr}] \times\left[-\frac{\tau\alpha_{2cr}\vartheta_2}{2(2\beta_2-\alpha_{2cr})}-\frac{3p_{2cr}}{4}\vartheta_2^3\right] - \frac{p_{2cr}}{4}\vartheta_0(\vartheta_0^2-\vartheta_2^2),$$

$$\vartheta_0\eta_0(\gamma_{1cr}^2A_1^2+\gamma_{2cr}^2A_2^2)-\gamma_{1cr}^2\vartheta_1\eta_1A_1^2-\gamma_{2cr}^2\vartheta_2\eta_2A_2^2 = \frac{\tau}{4}[(\alpha_{2cr}^2A_2^2-\alpha_{1cr}^2A_1^2)\vartheta_0^2+\alpha_{1cr}A_1^2\vartheta_1^2-\alpha_{2cr}A_2^2\vartheta_2^2] + \frac{1}{6}A_2^2(\vartheta_0^4-\vartheta_2^4)\left(\frac{\alpha_{2cr}}{8}-\beta_2\right)+\frac{1}{6}A_1^2(\vartheta_1^4-\vartheta_0^4) \times\left(\frac{\alpha_{1cr}}{8}-\beta_1\right). \quad \text{(A9)}$$

Since $\Delta=0$ it is necessary that the augmented matrix (obtained by adding the column of the right-hand side terms) has the same rank as the matrix of the coefficients. This condition can be written in the form $\Delta'=0$ where Δ' is the determinant of the square matrix obtained by substitution of the column of the right-hand side terms in place of whichever column of Δ. Then we substitute the first column of determinant Δ with the right-hand side terms of Eqs. (A9). The condition of vanishing determinant then reads

$$-\tau\left(\frac{\alpha_{1cr}}{\gamma_{1cr}^2}+\frac{\alpha_{2cr}}{\gamma_{2cr}^2}+\frac{t_1\alpha_{1cr}}{\gamma_{1cr}\sin(t_1\gamma_{1cr})\cos(t_1\gamma_{cr})} + \frac{t_2\alpha_{2cr}}{\gamma_{2cr}\sinh(t_2\gamma_{2cr})\cosh(t_2\gamma_{2cr})}\right) + \vartheta_0^2\left(\frac{3p_{1cr}t_1\gamma_{1cr}}{\sin(t_1\gamma_{1cr})\cos^3(t_1\gamma_{1cr})}-\frac{3p_{2cr}t_2\gamma_{2cr}}{\sinh(t_2\gamma_{2cr})\cosh^3(t_2\gamma_{2cr})}\right) + \vartheta_0^2\left(\frac{3p_{1cr}}{\cos^2(t_1\gamma_{1cr})}-\frac{3p_{2cr}}{\cosh^2(t_2\gamma_{2cr})}+2p_{1cr}-2p_{2cr}\right)=0, \quad \text{(A10)}$$

where $t_1=(x_0-x_1)$ and $t_2=(x_2-x_0)$ represent half of the layer thicknesses.

If we truncate the power expansion of Eq. (3) to the second order, we obtain, after integration, a system of three homogeneous linear equations in the angles ϑ_j. It is worth noting that the obtained system has the same matrix of coefficients of system (A9). The condition of vanishing determinant Δ at $H=H_{c1}$ leads to an implicit equation for the critical field

$$A_1\gamma_1\tan(t_1\gamma_{1cr})=A_2\gamma_2\tanh(t_2\gamma_{2cr}). \quad \text{(A11)}$$

Equation (A11) assumes the same form as that obtained in Refs. 2, 26, 37. Moreover, from this expansion to the lowest order, we can deduce the relations $\vartheta_0/\vartheta_1=\cos(t_1\gamma_{1cr})$ and $\vartheta_0/\vartheta_2=\cosh(t_2\gamma_{2cr})$.

APPENDIX B: INFINITESIMAL VARIATION OF MAGNETIZATION

From the definitions of the layer magnetizations

$$M_z=\frac{M_1\int_{x_1}^{x_0}dx\cos\vartheta+M_2\int_{x_0}^{x_2}dx\cos\vartheta}{(x_2-x_1)}=\frac{M_1I_1+M_2I_2}{(x_2-x_1)}, \quad \text{(B1)}$$

where M_1 and M_2 represent the saturation magnetization of the soft and hard layer, respectively, and with

$$I_1=\int_{x_1}^{x_0}dx\cos\vartheta\cong-\int_{x_1}^{x_0}\cos\vartheta\frac{d\vartheta}{\gamma_1\sqrt{\vartheta_1^2-\vartheta^2}}, \qquad I_2=\int_{x_0}^{x_2}dx\cos\vartheta\cong-\int_{x_0}^{x_2}\cos\vartheta\frac{d\vartheta}{\gamma_2\sqrt{\vartheta^2-\vartheta_2^2}} \quad \text{(B2)}$$

considering a power expansion truncated to the second order. The above integrals result

$$I_1=\left(1-\frac{\vartheta_0^2}{4\cos^2[\gamma_1(x_0-x_1)]}\right)(x_0-x_1) - \frac{\vartheta_0^2}{4\gamma_1}\tan[\gamma_1(x_0-x_1)],$$

$$I_2=\left(1-\frac{\vartheta_0^2}{4\cosh^2[\gamma_2(x_2-x_0)]}\right)(x_2-x_0) - \frac{\vartheta_0^2}{4\gamma_2}\tanh[\gamma_2(x_2-x_0)] \quad \text{(B3)}$$

and therefore the infinitesimal variation of the magnetization turns out to be

$$\delta M=M_s-M_z=\frac{M_1(x_0-x_1)+M_2(x_2-x_0)}{(x_2-x_1)}-M_z = \frac{\vartheta_0^2}{4(x_2-x_1)}\left\{\frac{M_1(x_0-x_1)}{\cos^2[\gamma_1(x_0-x_1)]}+\frac{M_1}{\gamma_1}\tan[\gamma_1(x_0-x_1)]\right\} + \frac{\vartheta_0^2}{4(x_2-x_1)}\left\{\frac{M_2(x_2-x_0)}{\cosh^2[\gamma_2(x_2-x_0)]} + \frac{M_2}{\gamma_2}\tanh[\gamma_2(x_2-x_0)]\right\}, \quad \text{(B4)}$$

where M_s is the saturation magnetization of the whole system. The reduced infinitesimal variation of M is then

$$\delta m=\frac{\delta M}{M_s}=\frac{\delta M(x_2-x_1)}{M_1(x_0-x_1)+M_2(x_2-x_0)} = \vartheta_0^2\frac{1}{4(M_1t_1+M_2t_2)}\times\left\{\frac{M_1t_1}{\cos^2[\gamma_1t_1]}+\frac{M_1}{\gamma_1}\tan[\gamma_1t_1] + \frac{M_2t_2}{\cosh^2[\gamma_2t_2]}+\frac{M_2}{\gamma_2}\tanh[\gamma_2t_2]\right\}=\vartheta_0^2\Gamma. \quad \text{(B5)}$$

APPENDIX C: GENERAL PROCEDURE FOR TRACING THE DEMAGNETIZATION CURVES

The problem of tracing the demagnetization curve implies the integration of Eq. (3) with the boundary conditions $(d\vartheta/dx)=0$ and $\vartheta=\vartheta_i$ for $x=x_i$ $(i=1,2)$ and $A_1(d\vartheta/dx)=A_2(d\vartheta/dx)$ and $\vartheta=\vartheta_0$ for $x=x_0$. This calculation involves elliptical integrals and is performed by numerical methods.

For a specific multilayer system, given a particular field H we have to find the angles ϑ_0, ϑ_1, ϑ_2 by solving the system given by the three equations

$$F_1(\vartheta_0,\vartheta_1,\vartheta_2,H) = \int_{\vartheta_0}^{\vartheta_1} \frac{d\vartheta}{\sqrt{\alpha_1(\cos\vartheta-\cos\vartheta_1)+\beta_1(\mathrm{sen}^2\,\vartheta-\mathrm{sen}^2\,\vartheta_1)}} - t_1 = 0,$$

$$F_2(\vartheta_0,\vartheta_1,\vartheta_2,H) = \int_{\vartheta_2}^{\vartheta_0} \frac{d\vartheta}{\sqrt{\alpha_2(\cos\vartheta-\cos\vartheta_2)+\beta_2(\mathrm{sen}^2\,\vartheta-\mathrm{sen}^2\,\vartheta_2)}} - t_2 = 0, \tag{C1}$$

$$F_3(\vartheta_0,\vartheta_1,\vartheta_2,H) = \alpha_1(\cos\vartheta_0-\cos\vartheta_1)+\beta_1(\mathrm{sen}^2\,\vartheta_0-\mathrm{sen}^2\,\vartheta_1) - \left(\frac{A_2}{A_1}\right)^2 [\alpha_2(\cos\vartheta_0-\cos\vartheta_2) + \beta_2(\mathrm{sen}^2\,\vartheta_0-\mathrm{sen}^2\,\vartheta_2)] = 0.$$

Using vector symbols we write $\mathbf{F}(\boldsymbol{\Theta})=0$, with $\mathbf{F}=(F_1,F_2,F_3)$ and $\boldsymbol{\Theta}=(\vartheta_0,\vartheta_1,\vartheta_2)$. We use the Newton-Raphson method, as described in the Numerical Recipes (see Ref. 48, p. 379), to find this solution. We start from a tentative value $\boldsymbol{\Theta}_{\mathrm{start}}$. In the neighborhood of any nonsingular $\boldsymbol{\Theta}$ the function $\mathbf{F}(\boldsymbol{\Theta})$ can be expanded in Taylor series

$$\mathbf{F}(\boldsymbol{\Theta}+\delta\boldsymbol{\Theta})=\mathbf{F}(\boldsymbol{\Theta})+\mathbf{J}\cdot\delta\boldsymbol{\Theta}+O(\delta\boldsymbol{\Theta}^2), \tag{C2}$$

where $\mathbf{J}=\partial(F_1,F_2,F_3)/\partial(\vartheta_0,\vartheta_1,\vartheta_2)$ is the Jacobian matrix of the system. By neglecting terms of order $\delta\boldsymbol{\Theta}^2$ and higher and by setting $\mathbf{F}(\boldsymbol{\Theta}+\delta\boldsymbol{\Theta})=0$ we obtain a set of linear equations for the corrections $\delta\boldsymbol{\Theta}$ that move each component function of the vector $\mathbf{F}$ closer to zero simultaneously, namely, $\delta\boldsymbol{\Theta}=-\mathbf{J}^{-1}\cdot\mathbf{F}$. The corrections are then added to the starting value $\boldsymbol{\Theta}_{\mathrm{new}}=\boldsymbol{\Theta}_{\mathrm{start}}+\delta\boldsymbol{\Theta}$ and the procedure is iterated until $|\mathbf{F}|$ is as small as we want, thus obtaining the desired value of $\boldsymbol{\Theta}$. With this value we can compute the magnetization M_z from Eq. (B1), once we have obtained $\vartheta(x)$ after integration of Eq. (3). We generally start from a value of the field H_0 very close to the nucleation field H_{c1} and from a tentative value of the angles $\boldsymbol{\Theta}_{\mathrm{tent}}$ given by the nucleation field equations [see Appendixes A, B and Eq. (7)]:

$$\vartheta_0=\sqrt{\frac{\chi_c(H_0-H_{c1})}{\Gamma M_s}},$$

$$\vartheta_1=\frac{\vartheta_0}{\cos(t_1\gamma_1)}, \tag{C3}$$

$$\vartheta_2=\frac{\vartheta_0}{\cosh(t_2\gamma_2)}$$

then we compute the right value of the angles $\boldsymbol{\Theta}_0$ (and the magnetization M_0) with the above-described procedure. Then we increase the field to H_1, take $\boldsymbol{\Theta}_0$ as the starting value and compute $\boldsymbol{\Theta}_1$ (and M_1), and so on. Each step we set $H_n=H_{n-1}+\mathrm{step}$ and compute $\boldsymbol{\Theta}_n$ using $\boldsymbol{\Theta}_{n-1}$ as the starting value. This way we are able to find M for each value of H, up to the reversal field H_{c2}. In correspondence of the second critical field H_{c2} an irreversible jump of the magnetization takes place. This means that a very small increase of the field H leads to very large changes in the values of the angles ϑ_0, ϑ_1, ϑ_2, that is, the first derivatives $d\vartheta_0/dH$, $d\vartheta_1/dH$, $d\vartheta_2/dH$ diverge. The derivatives are given by the vector equation

$$\begin{pmatrix} \frac{\partial\vartheta_0}{\partial H} \\ \frac{\partial\vartheta_1}{\partial H} \\ \frac{\partial\vartheta_2}{\partial H} \end{pmatrix} = -\left(\frac{\partial(F_1,F_2,F_3)}{\partial(\vartheta_0,\vartheta_1,\vartheta_2)}\right)^{-1}\frac{\partial(F_1,F_2,F_3)}{\partial H} = -\mathbf{J}^{-1}\begin{pmatrix} \frac{\partial F_1}{\partial H} \\ \frac{\partial F_2}{\partial H} \\ \frac{\partial F_3}{\partial H} \end{pmatrix}, \tag{C4}$$

where as usual $\mathbf{J}$ represents the Jacobian matrix of the system. Thus in order to get $d\vartheta_i/dH\to\infty$, we must seek the condition $J=0$. The step of the field H has to be repeatedly decreased while approaching H_{c2} (since the demagnetization curve becomes very steep) and we stop the procedure when the step has become small enough not to affect the value of the field within the set precision of $10^{-7}-10^{-8}$. By this point J has usually decreased by 3 or 4 orders of magnitude, and we consider this to be a convergence to zero.

[1] E. F. Kneller and R. Hawig, IEEE Trans. Magn. **27**, 3588 (1991).
[2] R. Skomski, J. Appl. Phys. **76**, 7059 (1994).
[3] R. Skomski and J. M. D. Coey, IEEE Trans. Magn. **29**, 2860 (1993).
[4] K. Mibu, T. Nagahama, T. Shinjo, and T. Ono, Phys. Rev. B **58**, 6442 (1998).
[5] B. Z. Cui and M. J. O'Shea, J. Magn. Magn. Mater. **256**, 348 (2003).

[6] S. Parhofer, J. Wecker, C. Kuhrt, and G. Gieres, IEEE Trans. Magn. **32**, 4437 (1996).
[7] C. J. Yang and S. W. Kim, J. Appl. Phys. **87**, 6134 (2000).
[8] M. Shindo, M. Ishizone, A. Sakuma, H. Kato, and T. Miyazaki, J. Appl. Phys. **81**, 4444 (1997).
[9] I. A. Al-Omari and D. J. Sellmyer, Phys. Rev. B **52**, 3441 (1995).
[10] E. E. Fullerton, J. S. Jiang, C. H. Sowers, J. E. Pearson, and S. D. Bader, Appl. Phys. Lett. **72**, 380 (1998).
[11] Shi-shen Yan, J. A. Barnard, Feng-ting Xu, J. L. Weston, and G. Zangari, Phys. Rev. B **64**, 184403 (2001).
[12] Shi-shen Yan, W. J. Liu, J. L. Weston, G. Zangari, and J. A. Barnard, Phys. Rev. B **63**, 174415 (2001).
[13] J. P. Liu, R. Skomski, Y. Liu, and D. J. Sellmyer, J. Appl. Phys. **87**, 6740 (2000).
[14] J. P. Liu, Y. Liu, and D. J. Sellmyer, J. Appl. Phys. **83**, 6608 (1998).
[15] J. P. Liu, Y. Liu, C. P. Luo, Z. S. Shan, and D. J. Sellmyer, J. Appl. Phys. **81**, 5644 (1997).
[16] E. E. Fullerton, J. S. Jiang, M. Grimditch, C. H. Sowers, and S. D. Bader, Phys. Rev. B **58**, 12193 (1998).
[17] E. E. Fullerton, J. S. Jiang, and S. D. Bader, J. Magn. Magn. Mater. **200**, 392 (1999).
[18] J. Kim, K. Barmak, M. De Graef, L. H. Lewis, and D. C. Crew, J. Appl. Phys. **87**, 6140 (2000).
[19] D. C. Crew, J. Kim, L. H. Lewis, and K. Barmak, J. Magn. Magn. Mater. **233**, 257 (2001).
[20] H. Kato, T. Nomura, M. Ishizone, H. Kubota, T. Miyazaki, and M. Motokawa, J. Appl. Phys. **87**, 6125 (2000).
[21] Jai-Lin Tsai, Tsung-Shune Chin, Jhy-Chau Shih, and Shi-Kun Chen, IEEE Trans. Magn. **35**, 3337 (1999).
[22] G. Asti, M. Carbucicchio, M. Rateo, and M. Solzi, J. Magn. Magn. Mater. **196–197**, 59 (1999).
[23] G. Asti, M. Carbucicchio, M. Ghidini, M. Rateo, and M. Solzi, J. Appl. Phys. **87**, 6689 (2000).
[24] M. Solzi, M. Ghidini, and G. Asti, in *Magnetic Nanostructures*, 1st ed., edited by H. S. Nalwa (American Scientific, Stevenson Ranch, CA, 2002), Vol. 1, Chap. 4, p. 124.
[25] E. Goto, N. Hayashi, T. Miyashita, and K. Nakagawa, J. Appl. Phys. **36**, 2951 (1965).
[26] F. B. Hagedorn, J. Appl. Phys. **41**, 2491 (1970).
[27] T. Leineweber and H. Kronmüller, J. Magn. Magn. Mater. **176**, 145 (1997).
[28] W. Andrä, IEEE Trans. Magn. **2**, 560 (1966).
[29] M. Amato, M. G. Pini, and A. Rettori, Phys. Rev. B **60**, 3414 (1999).
[30] H. Chang, Y. S. Lin, and A. Priver, J. Appl. Phys. **38**, 2294 (1967).
[31] Y. S. Lin and H. Chang, J. Appl. Phys. **40**, 604 (1969).
[32] R. F. Sabiryanov and S. S. Jaswal, Phys. Rev. B **58**, 12071 (1998).
[33] N. Hayashi and E. Goto, J. Appl. Phys. **37**, 3715 (1966).
[34] E. Goto, N. Hayashi, N. Honma, R. Kuroda, and T. Miyashita, Jpn. J. Appl. Phys., Part 1 **4**, 712 (1965).
[35] A. Aharoni, Phys. Rev. **119**, 127 (1960).
[36] C. Abraham and A. Aharoni, Phys. Rev. **120**, 1576 (1960).
[37] C. Abraham, Phys. Rev. **135**, A1269 (1964).
[38] T. Leineweber and H. Kronmüller, Phys. Status Solidi B **201**, 291 (1997).
[39] R. Skomski and J. M. D. Coey, Phys. Rev. B **48**, 15812 (1993).
[40] R. Skomski, J. Appl. Phys. **83**, 6503 (1998).
[41] S. Nieber and H. Kronmüller, Phys. Status Solidi B **153**, 367 (1989).
[42] G. J. Bowden, J. M. L. Beaujour, S. Gordeev, P. A. J. de Groot, B. D. Rainford, and M. Sawicki, J. Phys.: Condens. Matter **12**, 9335 (2000).
[43] S. Wüchner, J. C. Toussaint, and J. Voiron, Phys. Rev. B **55**, 11576 (1997).
[44] G. Asti, M. Solzi, and M. Ghidini, J. Magn. Magn. Mater. **226**, 1464 (2001).
[45] A. Aharoni, *Introduction to the Theory of Ferromagnetism*, Ith ed. (Clarendon Press, Oxford, 1996), Chap. 9.
[46] This is the mode if the limit of infinite slab is reached from an asymmetric configuration. In case of a rotation-symmetric system the reversal mode is the *curling* with the same nucleation field (see Ref. 45, p. 197).
[47] In the calculation we assume solutions with ϑ_1 and ϑ_2 having the same sign. In principle there should be also solutions in which the two angles have opposite sign. These are certainly less favored configurations, with higher energy or even unstable.
[48] *Numerical Recipes*, URL http://www.library.cornell.edu/nr/bookcpdf.html.
[49] A. Hubert and W. Rave, Phys. Status Solidi B **211**, 815 (1999).
[50] W. F. Brown, Phys. Rev. **124**, 1348 (1961).
[51] D. Chumakov, R. Schäfer, D. Elefant, D. Eckert, L. Schultz, S. S. Yan, and J. A. Barnard, Phys. Rev. B **66**, 134409 (2002).
[52] G. Asti, M. Ghidini, F. M. Neri, and M. Solzi, J. Magn. Magn. Mater. **272-276**, 650 (2004).
[53] S. T. Chui and Y. Yu, Phys. Rev. B **63**, 140419(R) (2001).
[54] R. Friedberg and D. I. Paul, Phys. Rev. Lett. **34**, 1234 (1975).
[55] H. Zijlstra, IEEE Trans. Magn. **6**, 179 (1970).
[56] M. Sawicki, G. J. Bowden, P. A. J. de Groot, B. D. Rainford, J.-M. L. Beaujour, R. C. C. Ward, and M. R. Wells, Phys. Rev. B **62**, 5817 (2000).
[57] A. Hubert and R. Schäfer, *Magnetic Domains* (Springer-Verlag, Berlin, 1998).